Research Paper

GEOSPHERE

GEOSPHERE, v. 16, no. 2

https://doi.org/10.1130/GES02118.1

13 figures; 1 table; 1 set of supplemental files

CORRESPONDENCE: mdechesne@usgs.gov

CITATION: Dechesne, M., Currano, E.D., Dunn, R.E., Higgins, P., Hartman, J.H., Chamberlain, K.R., and Holm-Denoma, C.S., 2020, A new stratigraphic framework and constraints for the position of the Paleocene–Eocene boundary in the rapidly subsiding Hanna Basin, Wyoming: Geosphere, v. 16, no. 2, p. 594–618, https://doi.org/10.1130/GES02118.1.

Science Editor: David E. Fastovsky

Received 1 February 2019
Revision received 1 October 2019
Accepted 9 December 2019

Published online 16 January 2020

A new stratigraphic framework and constraints for the position of the Paleocene–Eocene boundary in the rapidly subsiding Hanna Basin, Wyoming

Marieke Dechesne[1], Ellen D. Currano[2], Regan E. Dunn[3,4], Pennilyn Higgins[5], Joseph H. Hartman[6], Kevin R. Chamberlain[7], and Christopher S. Holm-Denoma[8]

[1]U.S. Geological Survey, Geosciences and Environmental Change Science Center, Box 25046, MS 980, Denver, Colorado 80225, USA
[2]Departments of Botany and Geology & Geophysics, University of Wyoming, 1000 E. University Avenue, Laramie, Wyoming 82071, USA
[3]Integrative Research Center, Field Museum of Natural History, 1400 South Lake Shore Drive, Chicago, Illinois 60605, USA
[4]Natural History Museums of Los Angeles County, La Brea Tar Pits & Museum, 5801 Wilshire Blvd, Los Angeles, California 90036, USA
[5]University of Rochester, Department of Earth and Environmental Sciences, 120 Trustee Road, Room 227, Rochester, New York 14627, USA
[6]Harold Hamm School of Geology & Geological Engineering, University of North Dakota, 83 Cornell Drive, Stop 8358, Grand Forks, North Dakota 58202, USA
[7]Department of Geology and Geophysics, University of Wyoming, 1000 E. University Avenue, Laramie, Wyoming 82071, *and* Faculty of Geology and Geography, Tomsk State University, Tomsk 634050, Russia
[8]U.S. Geological Survey, Geology, Geophysics, and Geochemistry Science Center, Box 25046, MS 973, Denver, Colorado 80225, USA

ABSTRACT

The Paleocene–Eocene strata of the rapidly subsiding Hanna Basin give insights in sedimentation patterns and regional paleogeography during the Laramide orogeny and across the climatic event at the Paleocene–Eocene Thermal Maximum (PETM). Abundant coalbeds and carbonaceous shales of the fluvial, paludal, and lacustrine strata of the Hanna Formation offer a different depositional setting than PETM sections described in the nearby Piceance and Bighorn Basins, and the uniquely high sediment accumulation rates give an expanded and near-complete record across this interval. Stratigraphic sections were measured for an ~1250 m interval spanning the Paleocene–Eocene boundary across the northeastern syncline of the basin, documenting depositional changes between axial fluvial sandstones, basin margin, paludal, floodplain, and lacustrine deposits. Leaf macrofossils, palynology, mollusks, $\delta^{13}C$ isotopes of bulk organic matter, and zircon sample locations were integrated within the stratigraphic framework and refined the position of the PETM. As observed in other basins of the same age, an interval of coarse, amalgamated sandstones occurs as a response to the PETM. Although this pulse of relatively coarser sediment appears related to climate change at the PETM, it must be noted that several very similar sandstone bodies occur with the Hanna Formation. These sandstones occur in regular intervals and have an apparent cyclic pattern; however, age control is not sufficient yet to address the origin of the cyclicity. Signs of increased ponding and lake expansion upward in the section appear to be a response to basin isolation by emerging Laramide uplifts.

INTRODUCTION

From the latest Cretaceous through early Eocene, the Hanna Basin in south-central Wyoming was one of the most rapidly subsiding basins of the Laramide foreland (Fig. 1; Roberts and Kirschbaum, 1995; Wroblewski, 2002; Jones et al., 2011). As a result, a thick, relatively continuous succession of shallow marine, fluvial, paludal and lacustrine strata is preserved in the center of the basin. This thick and continuous record allows to fill gaps in understanding the regional paleogeography and basin-fill history of nearby Laramide basins, such as the Denver Basin and North Park–Middle Park Basin, where sections are not as complete, and hiatuses are well documented within the section (Raynolds and Johnson, 2003; Cole et al., 2010; Dechesne et al., 2013). Earliest work focused on coal resources in the area (Veatch, 1907; Dobbin et al., 1929, Glass, 1980; Glass and Roberts, 1984; Flores et al., 1999a, 1999b) and showed either short sections for individual coal beds or generalized stratigraphic sections. The extensive work of Lillegraven (1994), Lillegraven and Snoke (1996), and Lillegraven et al. (2004) mostly focused on vertebrate occurrences and structure in The Breaks area and the northern basin margin. The occurrence of the Paleocene–Eocene Thermal Maximum (PETM, 56 Ma; Jaramillo et al., 2010) within the Hanna Basin had only generally been identified via mollusks, palynology, and isotopes (Kirschner, 1984; Flores et al.,1999a, 1999b; Higgins, 2012; Pew, 2014).

It has been hypothesized that climate change across the PETM caused changes in basin sedimentation by increased seasonal differences that produced larger flood events (Foreman et al., 2012; Foreman, 2014; Plink-Björklund, 2015). Terrestrial PETM sections in nearby Laramide basins (Foreman et al., 2012; Foreman, 2014) and in the Spanish Pyrenees (Colombera et al., 2017) have all been associated with amalgamated sheet sandstones. However, the Paleocene–Eocene deposits of the nearby Piceance and Bighorn Basins include predominantly fluvial deposits and floodplains with abundant paleosols (Foreman et al., 2012; Foreman, 2014; Kraus et al., 2015). Background sedimentation in the Hanna Basin is typified by a more ponded, fluvial to shallow lacustrine environment, thus allowing comparison and determination as to whether a similar sedimentation response is present across the PETM in a generally wetter depositional environment.

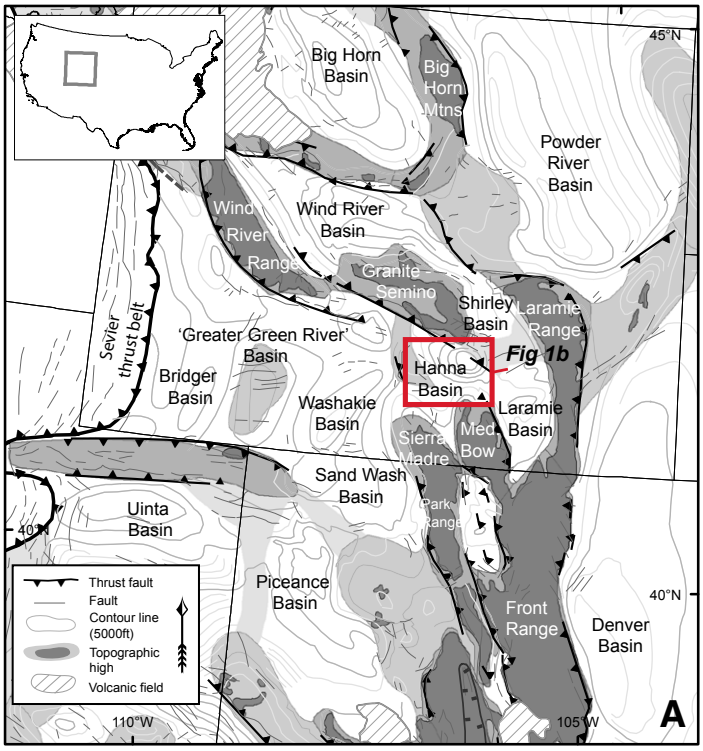

Figure 1. (A) Location map of the Hanna Basin with surrounding basins of the Laramide foreland outlined. Thick contour lines indicate depth to basement in 1500 m (5000 ft) intervals; thin contours are 300 m (1000 ft); base data from Rocky Mountain Association of Geologists (RMAG, 2014), tectonic GIS data from the Geologic Atlas of the Rocky Mountain Region (RMAG, 2014). Note depth to basement between Hanna Basin and surrounding basins. Red outline indicates study area and outline of Figure 1B. (B) Map of Paleocene–Eocene Hanna Formation outcrops (brown) and structural features (modified after Blackstone, 1993). Study area of Figure 3 indicated with white box; geologic unit contacts are generalized; plunging anticline (heavy gray arrow) represents uplift of Freezeout Mountains. The western margin of the Rawlins uplift separates the Hanna Basin from the Greater Green River Basin (Fig. 1A); the northern limit is the Sweetwater arch; the Simpson Ridge anticline forms the east boundary, and the Medicine Bow Mountains and Sierra Madre are the southern boundaries.

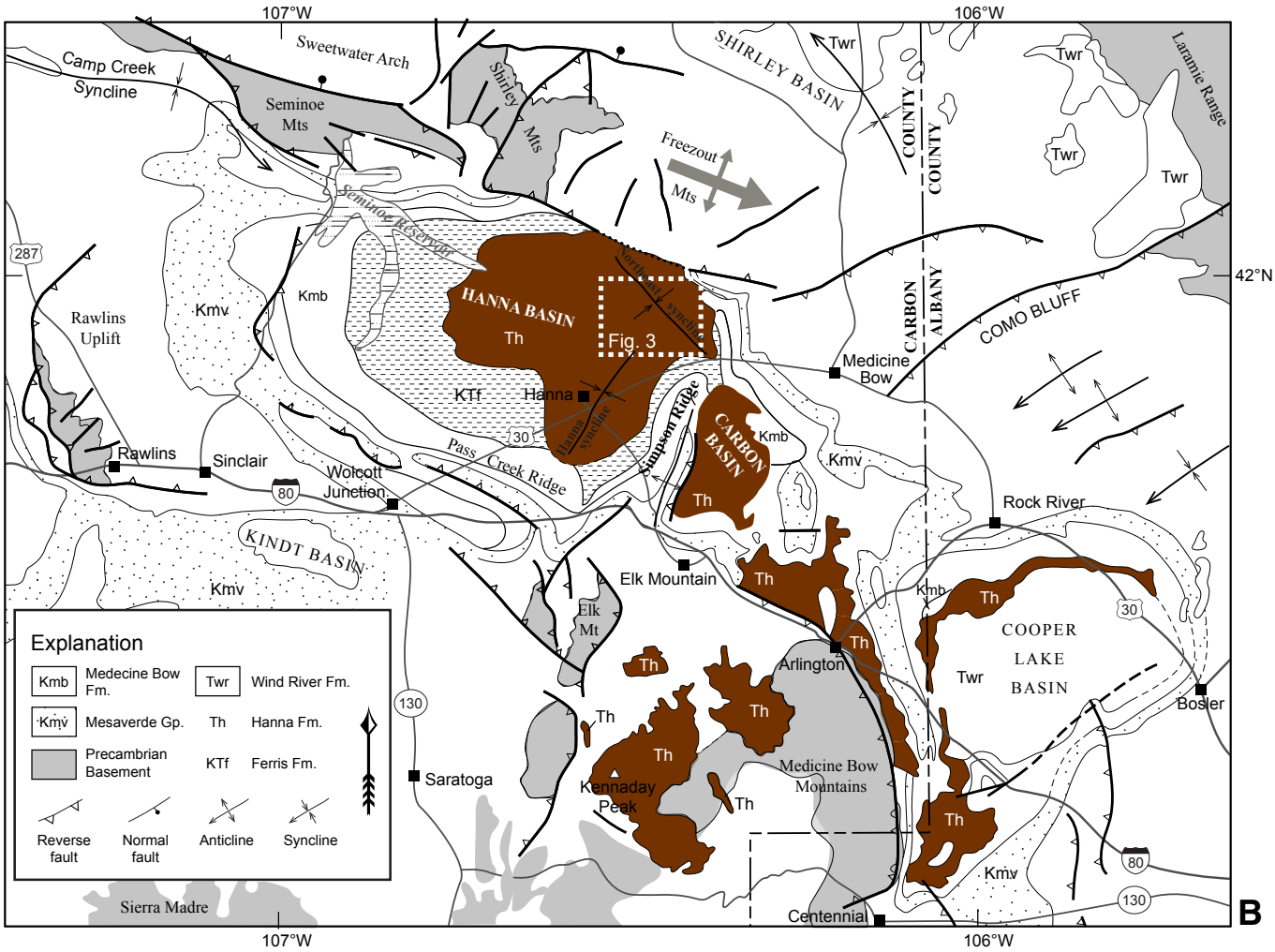

Geologic Setting

The Hanna Basin is especially noteworthy for its thick package of >12,500 m (40,000 ft) of Phanerozoic sedimentary strata (Fig. 1; Blackstone, 1993; Roberts and Kirschbaum, 1995; Lillegraven and Snoke, 1996; Wroblewski, 2003). Most rapid subsidence and sediment accumulation occurred from the Campanian through Eocene (Ypresian?) (Wrobleski, 2003) due to the Hanna Basin's position at the distal end of the Laramide flat slab present under the North American continent (Cross and Pilger, 1978; Dickinson and Snyder, 1978; Jones et al., 2011; Copeland et al., 2017).

The sedimentary succession of the Hanna Basin resembles nearby basins of Upper Cretaceous through Eocene age. However, because of its very high subsidence rates and sediment input, the Hanna Basin preserved a uniquely thick and relatively complete sedimentary record in its basin center. Main retreat of the Western Interior Seaway from this area in the late Maastrichtian is marked by the beach and shore-face deposits of the Fox Hills Sandstone. Leaf margin analysis and several marine incursions documented in the Upper Cretaceous Medicine Bow and Upper Cretaceous–Paleocene Ferris deposits suggest that the Hanna Basin remained at or near sea level until at least the early or middle Eocene (Dunn, 2003; Wroblewski, 2003, 2004; Boyd and Lillegraven, 2011; Cather et al., 2012; Lillegraven, 2015). Deposits progressively change from marginal marine and coastal plain to increasingly fluvial, paludal, and shallow lacustrine (Fig. 2). The Hanna Formation is most known for its coal beds and carbonaceous shales, which alternate with successions of siltstones, sandstones, and some conglomerates (Veatch, 1907; Bowen, 1918; Dobbin et al., 1929; Ryan, 1977; Glass, 1980; Flores et al., 1999a, 1999b; Wroblewski, 2002; Lillegraven et al., 2004). Formation and preservation of extensive coal beds indicate a densely vegetated landscape and high freshwater influx, causing extensive ponding and peat production that kept pace with the high accommodation and rapid burial (McCabe, 1984; Cecil, 1990; Bohacs and Suter, 1997; Flores et al., 1999b). The organic material that makes up the coals is interpreted to have accumulated in low-lying peat swamps tied into a fluvial system based on the relatively common centimeter-scale very fine sand and siltstone layers, which indicate intermittent fine-grained influx from distant rivers (McCabe, 1984; Pierce, 1996; Flores et al., 1999b).

Initially, the Hanna Basin was part of the Greater Green River Basin, later isolated into smaller subbasins by localized uplifts of the Laramide orogeny during the mid to late Paleocene (Fig. 1; Ryan, 1977; Blackstone, 1993; Perry and Flores, 1997; Secord; 1998; Kraatz, 2002; Wroblewski, 2003; Lillegraven, 2015; Smith et al., 2015b; Loope and Secord, 2017). The emergence of these uplifts influenced provenance and sedimentation patterns indicating predominantly local sources after this time (LeFebre, 1988; Blackstone 1993; Perry and Flores, 1997; Lillegraven et al., 2004; Peyton and Carrapa, 2013). Synsedimentary deformation within the Hanna and underlying Ferris Formations is well documented, especially along the basin's edges (Secord, 1998; Kraatz, 2002; Wroblewski, 2003; Lillegraven et al., 2004; Loope and Secord, 2017).

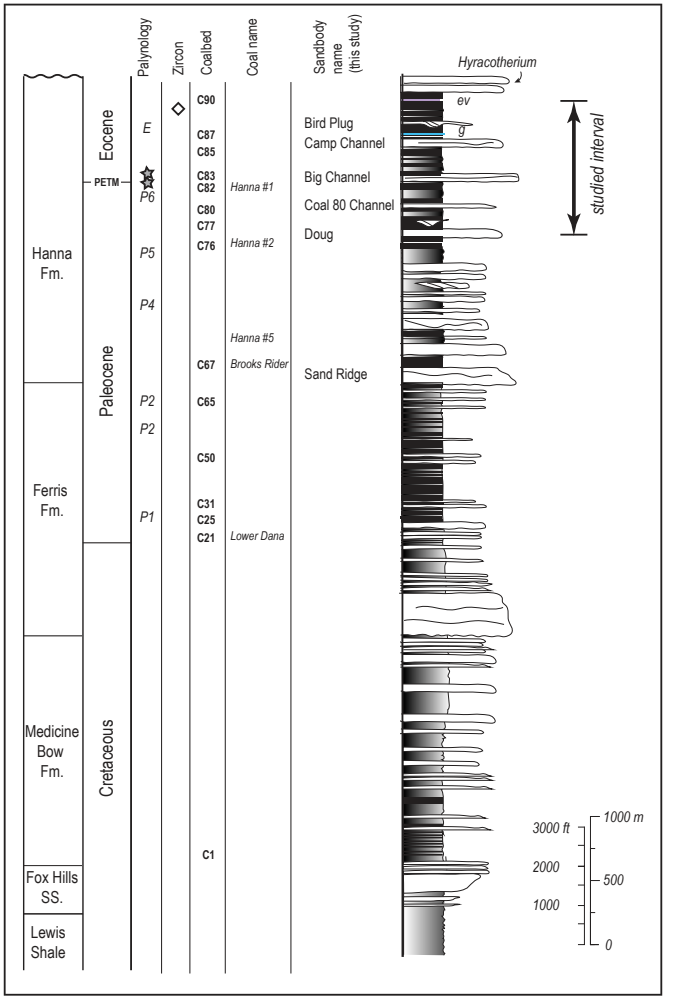

Figure 2. Generalized stratigraphic column showing the Upper Cretaceous through Eocene rocks of the Hanna Basin representing the retreat of the Western Interior Seaway, starting with the Lewis Shale, Fox Hills Sandstone and Medicine Bow, Ferris, and Hanna Formations. Coal beds (C1–C90) according to Dobbin et al. (1929), Glass and Roberts (1984), and Flores et al. (1999a, 1999b). Stratigraphic position of *Hyracotherium* and upper part of the Hanna Formation after Lillegraven et al. (2004). Interval of study indicated by arrow. Sand bodies discussed in text are named, as are coal beds of importance. Palynology (labeled as P-zones of Nichols and Ott, 1978) after Flores et al. (1999a, 1999b). Stars in Coal 82 upper and Coal 83 show first occurrences of *Platycarya*. Label *ev* indicates stratigraphic position of cm-thick gypsum evaporites, and *g* denotes the position of a distinct gastropod limestone bed (see Results and Discussion sections in text). The base of the Hanna Formation is gradational in the center of the basin, but not at the edges; the top of the Hanna Formation is erosional, and Miocene gravels overlie it (not shown in this figure). Note that this diagram is schematic and mostly based on the succession on the section in Hanna Draw, on the west side of the study area, rather than near the margins or The Breaks.

The base of the Hanna Formation is considered conformable with the Ferris Formation in the center of the Hanna Basin (Knight, 1951; Blackstone, 1993; Flores et al., 1999b). However, the basin margins show disconformable to angular contacts, because active underlying structures influenced accommodation and disrupted sedimentation (Knight, 1951; Love and Christiansen, 1985; Blackstone, 1993; Perry and Flores, 1997; Secord, 1998; Lillegraven et al., 2004; Loope and Secord, 2017). Hanna Formation reported thickness is therefore variable and greater in the center of the basin, and several maximum thickness values have been reported, ranging from ~3500 m (11,000 ft) to 2150 m (7000 ft) (Dobbin et al., 1929; Gill et al., 1970; LeFebre, 1988; Lillegraven and Snoke, 1996; Wroblewski, 2003; WOGCC, 2016).

General age information for the Hanna Formation was based on palynostratigraphy and intermittent occurrences of diagnostic mammalian fossils. Pollen zones P1 and P2 of Nichols and Ott (1978) are present in the Ferris Formation (Flores et al., 1999b; Dunn, 2003) along with Lancian and Puercan (Pu1–Pu3) mammals (Late Cretaceous–Paleocene, North American Land Mammal Age (NALMA); Eberle and Lillegraven, 1998a, 1998b). P3 pollen are found at the base of the Hanna Formation in the center of the basin, indicating onset of Hanna sedimentation in the mid-Paleocene or later, and P5 pollen are found at the basin margin in The Breaks corroborating uplift before and during deposition (Perry and Flores, 1997; Dunn, 2003; Lillegraven et al., 2004). A succession of vertebrate localities spans the latest Torrejonian (To3) through middle Tiffanian (Ti3) land mammal ages on the northeastern margin (Higgins, 2003), and a single tooth of *Hyracotherium grangeri* was found near the top of the Hanna Formation (Lillegraven et al., 2004), confirming a post-PETM Wasatchian age (early Eocene, NALMA) for its youngest beds (Gingerich and Clyde, 2001).

Paleoclimatic Setting

The North American continental interior was warm and equable, with minimal frost, during the Paleocene and early Eocene (Wing and Greenwood, 1993). Globally, temperatures gradually warmed across this interval to a sustained Cenozoic maximum from 52.6 to 50.3 Ma (Zachos et al., 2008; Payros et al., 2015). The PETM, an abrupt global perturbation to the carbon cycle at the Paleocene–Eocene boundary, had a profound effect on Earth surface systems (McInerney and Wing, 2011). In less than 20,000 years, thousands of petagrams of isotopically light carbon were released into the atmosphere and ocean as evidenced by a 3–5 per mil (‰) global decrease in carbon isotope values, referred to as a negative carbon isotope excursion (CIE) (Kennett and Stott, 1991; Koch et al., 1992; Cui et al., 2011; Bowen et al., 2015).

Independent paleoclimate proxies document global warming of 5–8 °C accompanying this carbon release (McInerney and Wing, 2011). Bowen et al. (2004) and Winguth et al. (2010) proposed that increased pCO_2 and temperature intensified the hydrologic cycle and enhanced monsoonal circulation in the Western Interior during the PETM. PETM vegetation records exhibit varying degrees of floral change, with most records for temperate and high latitudes showing an abundance decrease in conifers and increase in thermophilic angiosperms (Wing and Currano, 2013). Changes to the hydrologic cycle and vegetation structure during the PETM, in turn, impacted river systems and sediment accumulation in the Bighorn and Piceance Basins (Foreman et al., 2012; Foreman 2014).

FIELD STUDIES AND ANALYTICAL METHODS

Stratigraphy

Detailed stratigraphic sections were measured on both flanks of the northeast syncline from which a stratigraphic framework for the upper Hanna Formation was developed (Figs. 3 and 4; Supplement S1[1]). Two of the measured sections span the entire studied interval: one in Hanna Draw (~1250 m; ~4100 ft) on the west limb of the syncline and one on the east limb, in The Breaks (TB; 940 m; 3083 ft). The Hanna Draw composite section was measured southeast of Hanna Draw road (HD; Fig. 3). The Breaks section approximately corresponds with the location of Leg 17, originally measured by Lillegraven (1994), and later worked by Higgins (2012) and Pew (2014), who both focused on identifying the PETM in The Breaks by isotopes and palynology. The Beer Mug Vista (BMV) section (278 m; 912 ft) captures proximal-to-distal facies relations from near the basin margin to the relatively more distal and shallow lacustrine section in The Breaks. The Big Channel Lateral (BCL; 193 m; 633 ft) and Big Channel Axis (BCA; 82 m; 270 ft) sections capture lateral changes between across the PETM section in Hanna Draw.

The stratigraphic framework was tied to the coal-bed nomenclature of Dobbin et al. (1929); this framework was established in Hanna Draw near our measured section and was maintained by later workers, so that previous work could be more easily integrated (e.g., Glass, 1980; Glass and Roberts, 1984; Flores et al., 1999a, 1999b). Dobbin et al. (1929) did not extend correlations toward the active basin margins because increased clastic input interfingers with the paludal deposits, and coal beds are not as well developed. However, in the center of the basin, coal beds and carbonaceous shale intervals are laterally continuous over at least 5–10 km. Dobbin maps only the thickest and laterally most continuous coal beds and shales (Coals 78, 79, 80, 81, 87, 88, and 89) across the also faulted syncline between Hanna Draw and The Breaks. To enhance correlation certainty, this study did not exclusively use coal beds and carbonaceous shales, but also paleobotany results and stratigraphic marker beds, such as the gastropod limestone bed within Coal 87, aerial photography (NAIP, 2012), Google Earth, and walking beds laterally. The here-developed framework spans the interval between Coal 77 and an originally unnamed coal bed just above Coal 89 of Dobbin et al. (1929), labeled Coal 90 here (Figs. 2 and 4). It is important to note that Lillegraven et al. (2004) mapped 600 additional meters of increasingly more sand-rich strata above Coal 90 in the Hanna Formation that were not incorporated in this framework.

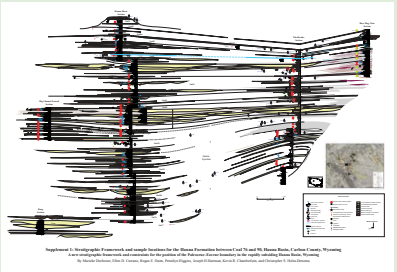

[1]Supplemental Materials. Supplement S1: Full stratigraphic diagram for the upper Hanna Formation between Coal 77 and 90 between Hanna Draw and The Breaks. Locality and sample data are plotted. Supplement S2a: Methods, figures and results for the thermal ionization mass spectrometry (TIMS) and laser ablation–inductively coupled mass spectrometry (LA–ICPMS) zircon analysis. Supplement S2b: Data tables for the laser ablation zircon analysis. Supplement S3: Tables listing bulk carbon isotope data conducted for this study. Please visit https://doi.org/10.1130/GES02118.S1 or access the full-text article on www.gsapubs.org to view the Supplemental Materials.

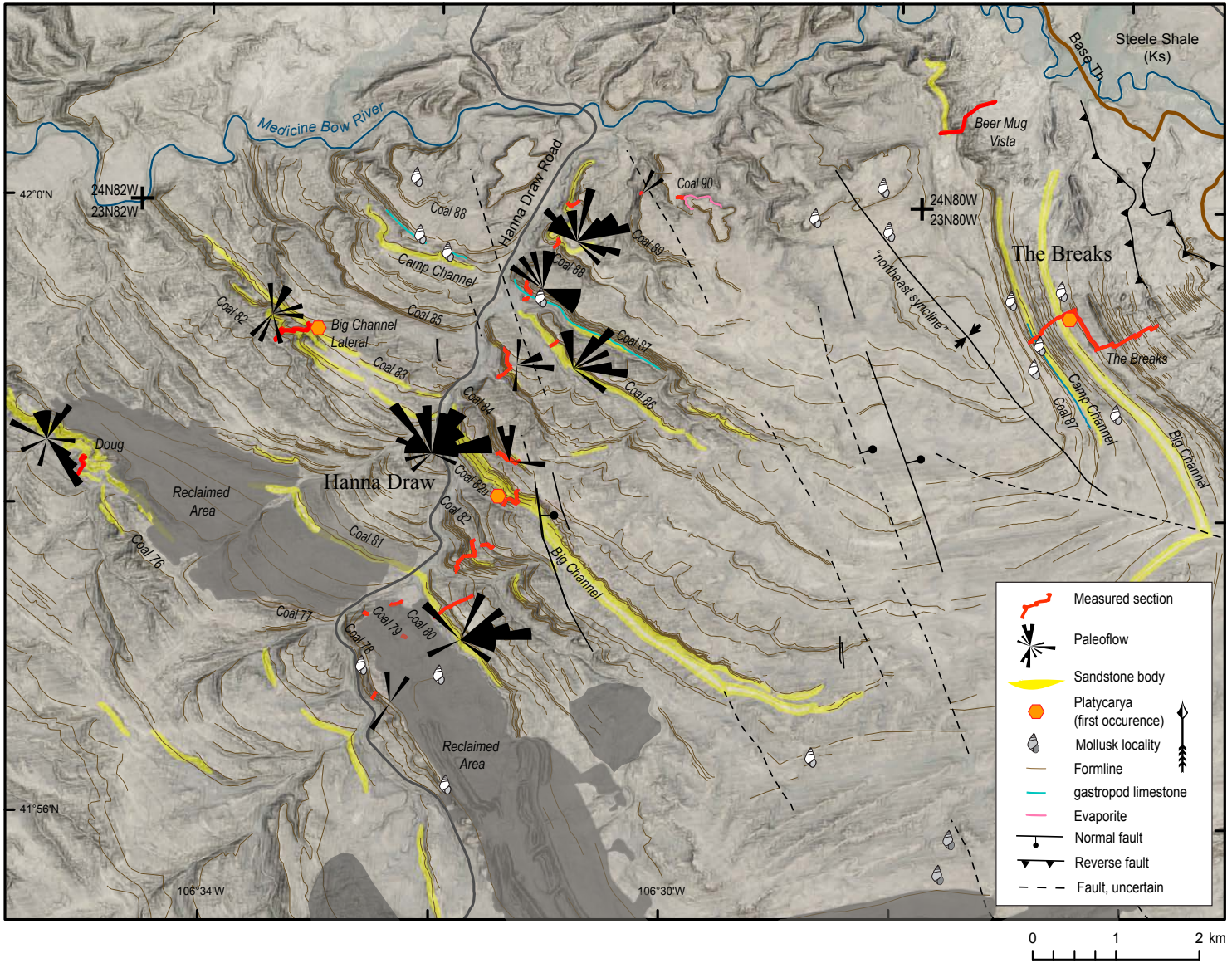

Figure 3. Map of measured sections between Coal 77 and 90 and major sandstone bodies (in yellow) within the Hanna Formation (indicated as Th).

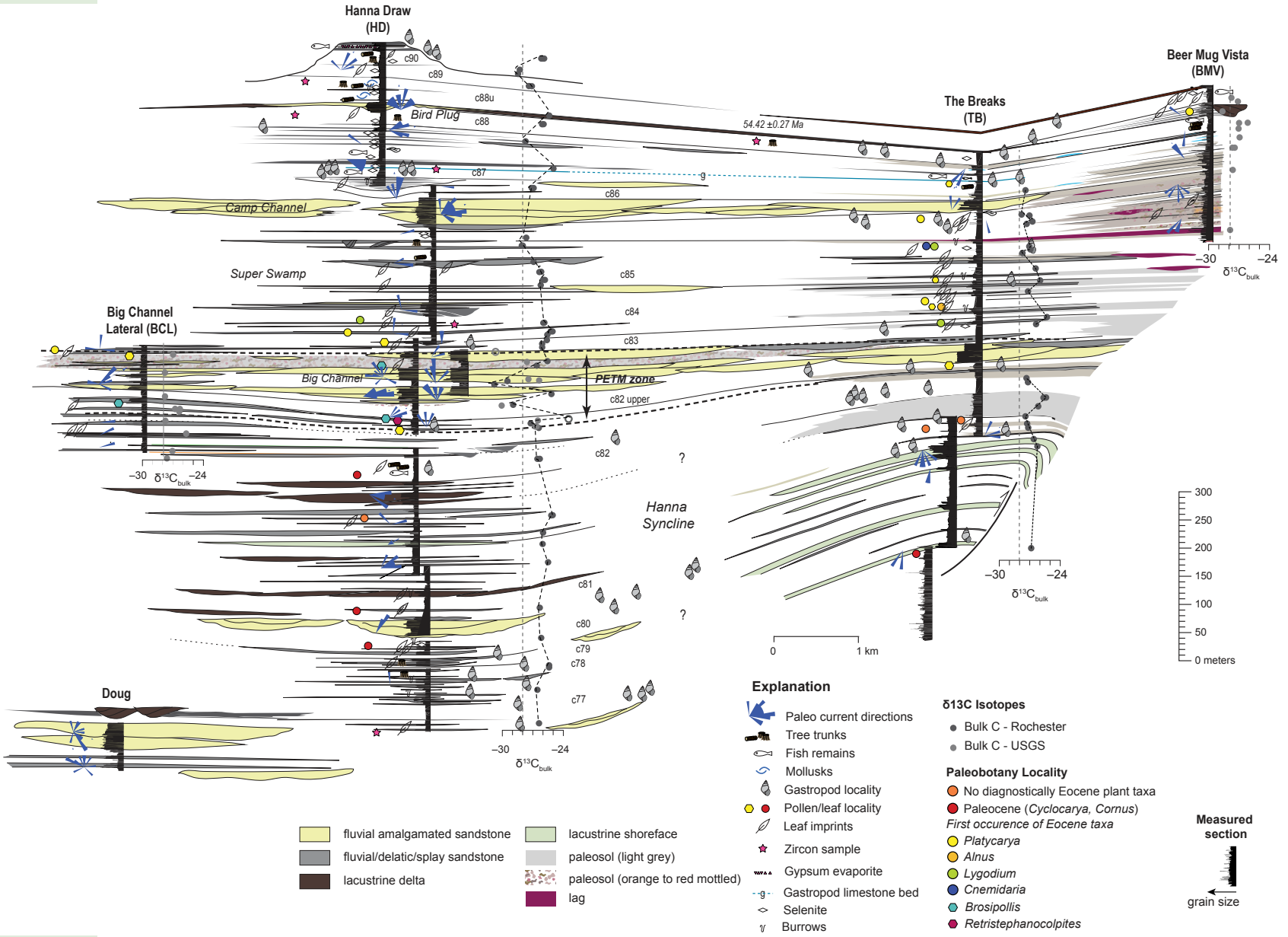

Figure 4. Stratigraphic framework for the upper Hanna Formation between Coal 77 and 90 (detailed version with all localities in Supplement S1 [text footnote 1]). Measured sections are composite, and their locations are indicated on Figure 3. Paleocene–Eocene Thermal Maximum (PETM) interval is indicated by arrows between Coal 82 upper and Coal 83. Bulk $\delta^{13}C_{org}$ isotopes plotted as gray dots and black dashed line through data points. Question marks indicate uncertainty in correlations.

Paleobotany

Organic-rich sandstone, siltstone, mudstone, and shale beds along Hanna Draw and in The Breaks were surveyed for plant macrofossils. Occurrences of biostratigraphically indicative taxa were recorded and plotted on the stratigraphic sections. Of particular importance are the early Eocene index taxa *Platycarya* (Juglandaceae), *Salvinia preauriculata* Berry (Salviniaceae), *Lygodium kaulfussi* Heer (Schizaeaceae), and *Cnemidaria magna* (Cyatheaceae) (Brown, 1962; Nichols and Ott, 1978; Manchester and Zavada, 1987; Wing, 1998). The occurrence of *Cyclocarya* fruits and *Cornus swingii* leaves in the study area indicates a Paleocene age (Manchester, 1987; Manchester et al., 2009). Voucher specimens of identifiable plant parts from each locality are curated at the University of Wyoming Geological Museum. GPS coordinates are available from the authors, pending permission from the Bureau of Land Management (BLM) or property owner.

Palynological sampling was undertaken to determine the age of strata in the measured sections based on the well-established Paleocene–Eocene palynostratigraphic scheme (P-biozones) of Nichols and Ott (1978) and Nichols (2003). Samples were collected from fine-grained units including carbonaceous shales and coals. Palynological preparations were made using two different methods: (1) standard palynological preparations were performed by Global Geolabs Ltd. in Medicine Hat, Alberta, Canada; and (2) HF-free preparations (following O'Keefe and Eble, 2012) were performed by Jen O'Keefe at Morehead State University, Morehead, Kentucky, USA. Prepared microscope slides were scanned using light microscopy, and the occurrences of diagnostic pollen grains were noted. To pinpoint the PETM interval, first appearance data were recorded for known PETM and Eocene taxa described from other Western Interior basins and the Gulf Coast, USA (e.g., Harrington, 2003a, 2003b).

Invertebrate Fossils–Continental Mollusks

The study of Hanna Formation continental mollusks is part of a larger project to revise and evaluate taxonomy and biostratigraphy of western United States Cretaceous and Paleogene taxa[2]. An evaluation of previous continental molluscan records from the Ferris and Hanna Formations by Lesquereux (1874), Glass (1980), and Kirschner (1984) is supplemented with new, stratigraphically controlled specimens to confirm the Paleocene–Eocene boundary, to refine early Eocene stratigraphy and enhance paleoenvironmental interpretations. Study included examination of material at the Smithsonian Institution (Department of Paleobiology, U.S. National Museum of Natural History, Washington, D.C.), U.S. Geological Survey (USGS, Denver, Colorado), and the University of Wyoming Geological Museum (Laramie, Wyoming). Species of interest to determine the Paleocene–Eocene boundary include *Micropygus*, *Elimia*, and *Paludotrochus*.

[2]J.H. Hartman has maintained a North American continental molluscan locality numbering system (L-numbers [Lnos]) since 1978. Lnos reported in Supplement S1 text (footnote 1).

Bulk Organic Carbon

Bulk organic carbon samples for each major coal or lignite interval were collected while measuring section. Each sample was pulverized in the lab, after which the sample was treated with hydrochloric acid to remove siderite and carbonate overprints. Samples were then dried, weighed, and analyzed by mass spectrometer for $\delta^{13}C_{org}$. Two labs were used for processing and analyzing. About half the samples were processed by the Stable Isotope Ratios in the Environment, Analytical Laboratory (SIREAL) at the University of Rochester, New York, using a DeltaPlus XP mass spectrometer interfaced to a Costech 1410 Elemental Analyzer via a Thermo Electron Conflo III. All analyses were reported in permil (‰) relative to VPDB (Vienna Pee Dee Belemnite) and normalized (Coplen, 1994) so that the carbon isotopic value of standard reference material (SRM) 8539 is –29.73‰, of SRM 8542 is –10.45‰, and of SRM 8541 is –16.05‰ following the methods outlined in Higgins (2012). The other samples were processed at the USGS in Lakewood, Colorado, following Johnson et al. (2018) using a Carlo Erba NC2500 elemental analyzer coupled to a Micromass Optima isotope ratio mass spectrometer (IRMS) via a custom-built, open-split interface. All $\delta^{13}C_{org}$ samples were standardized to VPDB.

Zircon Geochronology

Several centimeter-scale, white, weathered, clay-rich mudstones to fine-grained sandstone beds, suspected of being ash beds or tonsteins, are present within the coal and carbonaceous shale intervals. Samples were collected for isotope dilution–thermal ionization mass spectrometry (ID-TIMS) U-Pb zircon dating to better constrain the age of the Hanna Formation and specifically the absolute age of strata interpreted to represent the PETM. Zircons were concentrated from these beds by ultrasonic deflocculation (mudstones), standard crushing (sandstones), and density and magnetic separations. Each sample yielded zircons with a variety of morphologies, including minor populations of mechanically rounded grains that are interpreted to be older, detrital zircons. Zircons were dated by laser ablation–inductively coupled mass spectrometry (LA-ICPMS) as a screening tool and by high-precision, chemical abrasion (adapted from Mattinson, 2005), isotope dilution, thermal ionization mass spectrometry (CA-ID-TIMS). Dating efforts by TIMS focused on euhedral grains with sharp crystal vertices, elongate tips, and longitudinal bubble tracks, which are diagnostic of volcanic, ash-fall origin. A detailed description of TIMS and LA-ICPMS analysis techniques is in Supplement S2a (footnote 1).

RESULTS

Stratigraphy

The stratigraphic framework documents facies changes across the study area and allowed positioning of all sample, paleobotany, and mollusk localities

leading to a more precise identification of the PETM (Fig. 4; detailed framework with fossil and sample localities in Supplement S1 [footnote 1]). Sandstone, shale, and coal intervals are typical for fluvial, paludal, and lacustrine environments, and lateral facies changes are gradational and influenced by relative position within the basin, e.g., basin-axial (Hanna Draw Section [HD]), distal to marginal lacustrine near the east side of the study area (The Breaks Section [TB]), or basin margin (Beer Mug Vista [BMV]). Lithofacies are summarized in Table 1.

Fluvial Sandstones

The largest sandstone bodies within our study area, here informally named "Big Channel" and "Camp Channel," can be traced between Hanna Draw and more distally into The Breaks (Figs. 3 and 4). They contain multiple amalgamated and internally incised channel sandstone bodies with meter-scale barforms, low-angle, planar, trough, and climbing-dune cross stratification. Soft-sediment deformation of sedimentary structures is relatively common, especially in the upper parts of the channels and corroborates rapid deposition (Fig. 5). Coarsest clasts (cobbles up to 10 cm) are found in the Big Channel section (BC) in Hanna Draw. Clasts match compositions of the units present in nearby uplifts, ranging from chert (Cloverly Formation), angular, white to light-gray shale parts (Mowry Shale), quartz sandstones with well-rounded frosted grains (Tensleep Formation), and occasional granitic or metamorphic basement clasts.

In Hanna Draw, Big Channel is not one channel but a clustering of three axial channel complexes of each 10–20 m (30–65 ft) thick, separated by equally thick intervals of carbonaceous shales with root casts, slickensides, and light-gray to orange and orange-to-red mottled paleosols. The orange-to-red paleosols are best developed in the fine-grained sand, silt, and shale deposits between 121 and 136 m (stories 2 and 3) in BC in Hanna Draw and are not common in the rest of the section in Hanna Draw. Lateral offsets between individual channel axes are between ~30 and 125 m (100–400 ft). In BCL and away from its axis, Big Channel complex splits up into multiple individual sandstone bodies that are less coarse, indicating that the location of BC is more axial (Fig. 4).

Big Channel's distal expression in The Breaks (Fig. 6A) is at least 34 m thick (110 ft; top not exposed) and at least 3 km wide, of yellow sandstone with clasts up to 4 cm (1.5 in) diameter, abundant crossbedding (Fig. 6B), and soft-sediment deformation. It is correlated to Hanna Draw based on paleobotanical information, overall stratigraphic patterns, and lithologic characteristics. Camp Channel, almost equally as large as Big Channel, is also correlative into The Breaks. It is made up of similar sedimentary features; however, soft sediment deformation is even more abundant, as are up to 2 m concretions (Fig. 6C).

In contrast, between Coal 88 and 88 upper and in general vertical sequence with the occurrence of the other larger sandstone complexes, is an 18-m-thick sandstone unit encased carbonaceous shales (Bird Plug Fig. 2; Figs. 5 and 7). This sandstone is also correlative between Hanna Draw and BMV; however, it is only expressed as a thin, rippled sandstone bed in TB (at 505 m; Supplement S1 [footnote 1]). The carbonaceous shales both below and above this sandstone contain large metasequoia tree trunks and dark-brown mudstones with fish scales (Fig. 7C). Internal foresets dip in multiple directions, and climbing ripples are abundant. Coarse basal pebble lags are absent; however, soft clast rip-up lags and mud-injection features are common. Oversteepened bedding (Fig. 7D), rotated blocks, and slumping suggest a less consolidated stratum and possibly deeper water depth more typical for a (lacustrine-) deltaic than fluvial origin. Distally, foresets become unidirectional more distally and resemble the tangential foresets common between Coal 81 and 82 (Figs. 7E and 7F). These features suggest distal conditions compared with the other large amalgamated sandstones, likely by the increasingly lacustrine nature of the section above Coal 87.

Large sandstone complexes with similar facies and channel dimensions occur at regular intervals in the Hanna Formation—for example, between Coal 80 and 81 and Coal 76 and 77 (called Doug; Fig. 2) and at the base of the Hanna Formation (Sand Ridge, between Coal 66 and 67, Fig. 2). These pulses of relatively coarse sediment appear repetitive. Comparison of internal lithofacies and dimensions between these sandstones shows that there is an overall decrease in large-scale, high-energy bedforms and increase in ripples and soft sediment deformation within the channels (Fig. 8). The sandstones of Big Channel do stand out as a non-amalgamated cluster of channels and coarser clasts and larger bedforms than observed in the channels directly below.

Isolated channels with accretion sets, abundant climbing ripples, and sometimes coarse to gravelly lags are common within coal and carbonaceous shale intervals (most commonly between Coals 77 and 79 and Coals 83–85 in Hanna Draw). Channel sizes vary between 1 and 5 m in thickness, and widths range from 8 to 85 m. They are associated with laterally continuous, tabular sandstones with internal scouring and climbing ripples encased in carbonaceous shale intervals that are interpreted as splays and splay channels.

Basin Margin

Closer to the basin margin, at Beer Mug Vista (BMV; Fig. 4), coarse sandstone-to gravelly beds of 10–30 cm with common angular clasts of Mowry Shale, siderite, and iron oxide–cemented sandstone occur (Fig. 9A). These beds are especially common in the lower half of BMV, but some of them extend south toward TB. Coarse grain size and angularity indicate a higher depositional gradient and limited transport distance because BMV is presently (after Laramide shortening) ~6 km from the Freezeout Mountains, the northern basin margin. These shallow lag deposits might represent fan rather than true fluvial deposits. The iron oxide–cemented sandstone clasts appear similar to ones described in the nearby Carbon Basin by Loope and Secord (2017), who proposed that these concretions originally formed as siderite nodules in the Ferris Formation. These nodules were then exposed by erosion from active uplift by underlying structures and resedimented in the Hanna Formation. Dips within BMV shallow upward and range from 30° at its base to 15° near its top, which supports the presence of an actively growing structure (Fig. 9B).

Table 1. Lithofacies for the upper Hanna Formation (Coal 77 - Coal 90)

General Depositional Environment		Facies name	Description (sedimentary texture and structures)	Thickness	Interpretation
Lacustrine		Evaporite	Bedding-parallel layers of gypsum (only encountered in coal 90)	1-2 cm thick	Restricted to evaporative lake (Smith et al., 2008)
		Cone in cone	Cone-in-cone structures of siderite, within coalbed (only encountered in The Breaks, TB)	4 cm thick	Shallow lake to swamp
		Carbonate-cemented mudstone	Finely-laminated, carbonate-cemented mudstone (avg 59% $CaCO_3$, Davis, 2006)	20-100 cm thick	Restricted lake
		Carbonate-cemented fine to very fine sandstone	Carbonate-cemented fine to very fine sandstone, beds often have wave-rippled tops, apparent biologic film overprint (Smith et al., 2015a)	5-30 cm thick	Restricted lake
		Gastropod limestone	Gastropod biowackestone, thinly laminated, organic drapes (Coal 87, The Breaks and Hanna Draw)	8-10 cm thick	Shallow freshwater lake (Bowen et al., 2008), littoral lacustrine
		Burrowed sandstone	Horizontal, mm- to cm-scale bedding-parallel burrows usually developed on thin-bedded, fine-to very fine ripple beds. Common below carbonaceous shale or coal intervals Burrows can be vertical or horizontal. 2-8-cm-thick vertical crayfish burrows in cross-bedded sandstones or in sandstones with minor paleosol developement.	Up to 30 cm thick	crayfish (shallow lake to fluvial, fluctuating water table, Hasiotis and Honey, 2000)
		Swaley to parallel bedded sandstone	Flaggy-weathered, swaley cross-bedded fine-to-very fine sandstone.	10-25 cm thick	Lake (above wave base)
		Wave-rippled sandstone	Isolated symmetrical ripples (on tops of beds) to stacked wave ripples	cm scale - 40 cm	Wave-reworked distal splay (in standing water) or lake
	Paludal and floodplain	Dark-brown carbonaceous shale	Dark-brown carbonaceous shale, often with plant material and\or fish and insect fragments	Varies, up to several meters	Swamp to lake
		Coal	Black, vitrous coal and klinker (burned coal)	Varies (up to meters - mined)	Swamp
		Dark-gray carbonaceous shale	Dark gray carbonaceous shale, often with tree trunks, leave casts or other plant material, and gypsum crystals	Varies, up to several meters	Swamp
		Light-gray, silty shale (immature paleosol?)	Light-to-medium grey, crumbly and blocky siltstone, mudstone and carbonaceous shale, often with slickensides and root casts	Varies, up to 1.5m	Swamp
		Sandy light-gray shale (immature paleosol)	Sandy, light-gray shale, structureless, light-to-medium grey, crumbly and blocky sandstone and siltstone, often with slickensides and root casts.	Varies, up to 1.5m	Swamp
		Laminated siltstone	mm-scale laminated siltstone and carbonaceous shale	Variable	Floodplain and distal splay
		Orange-to-red paleosol	Mottled, silty, fine to medium sandstone	Variable	Better drained, higher grounds
	Deltas and splays	Graded beds	Graded beds (to Bouma sequence Tbcde, Tcde)	2?-10 cm	Sediment gravity flow off delta front (in Coal 77, above Doug)
		Rippled sandstone	Current ripples, usually isolated or in trains	cm scale - 40 cm	Distal splay or lake
		Climbing rippled sandstone	Climbing ripples in fine sandstone	10 - 150 cm	Rapid deposition, high suspended load fluvial channel edge, splay or delta
		Very fine to heterolithic sandstone and/or siltstone	Very fine mm-scale alternations between parallel laminated very fine sand, siltstones and carbonaceous shales	5 - 50 cm	Waning - fluvial channel or splay
		Parallel-laminated sandstone	mm-scale parallel laminated sandstone	5 - 100 cm	Floodplain
		Small-scale scours and cross-bedded sandstone	Small-scale scours and fill, sometimes with through cross beds up to 50 cm, or scours often filled with climbing ripples	20 - 50 cm	Splay channel
	Fluvial	Structureless or cryptically laminated sandstone	Structureless, fine to medium-grained sandstone	Up to 3 m	Bioturbation, soft-sediment deformation fluvial
		Soft-sediment deformed sandstone	Convolutely bedded fine to medium sandstone	Up to 3 m	Rapid deposition, fluvial
		Trough-cross stratification (some occasional pebble lining on foresets)	Trough-cross bedded fine to medium sandstone	Up to 1.5 m bed sets	Rapid deposition, high suspended load deposition in channels
		Climbing dune cross stratification	Climbing dunes in upper fine to upper medium sandstone		
		Planar tabular cross stratification	Planar tabular cross bedding of 15-80 cm sets in medium- fine sandstone	In stacked sets up to 3m	Rapid deposition, channels
		Low-angle, large-scale barforms	Low-angle to parallel cross bedding in upper fine to coarse sandstone, often contain ripples on foresets	Up to 1.5 m bed sets	Barforms, channels
		Mud clast conglomerate	Conglomerate composed of mud, siltstone or coal rip-up clasts	Up to 50 cm	Bank collapse, or rip-up of underlying soft material at channel base or margin
		Gravel, pebble or cobble conglomerate	Conglomerate made up of gravel, pebbles, and/or cobbles, comprising angular Mowry Shale, rounded chert from the Cloverly Fm. and sandstone clasts with frosted grains of Tensleep Fm.	Up to 50 cm	Lag deposit, channel base
		Coarse-grained, angular sandstone lag with siderite concretions	Iron-oxide-cemented fine to coarse sandstone with recycled siderite concretions, angular clasts of Mowry Shale, and chert derived from Cloverly Fm.	Up to 50 cm	Lag deposit (fan delta), near basin margin occurs at Beer Mug Vista section (Loope and Secord, 2017)

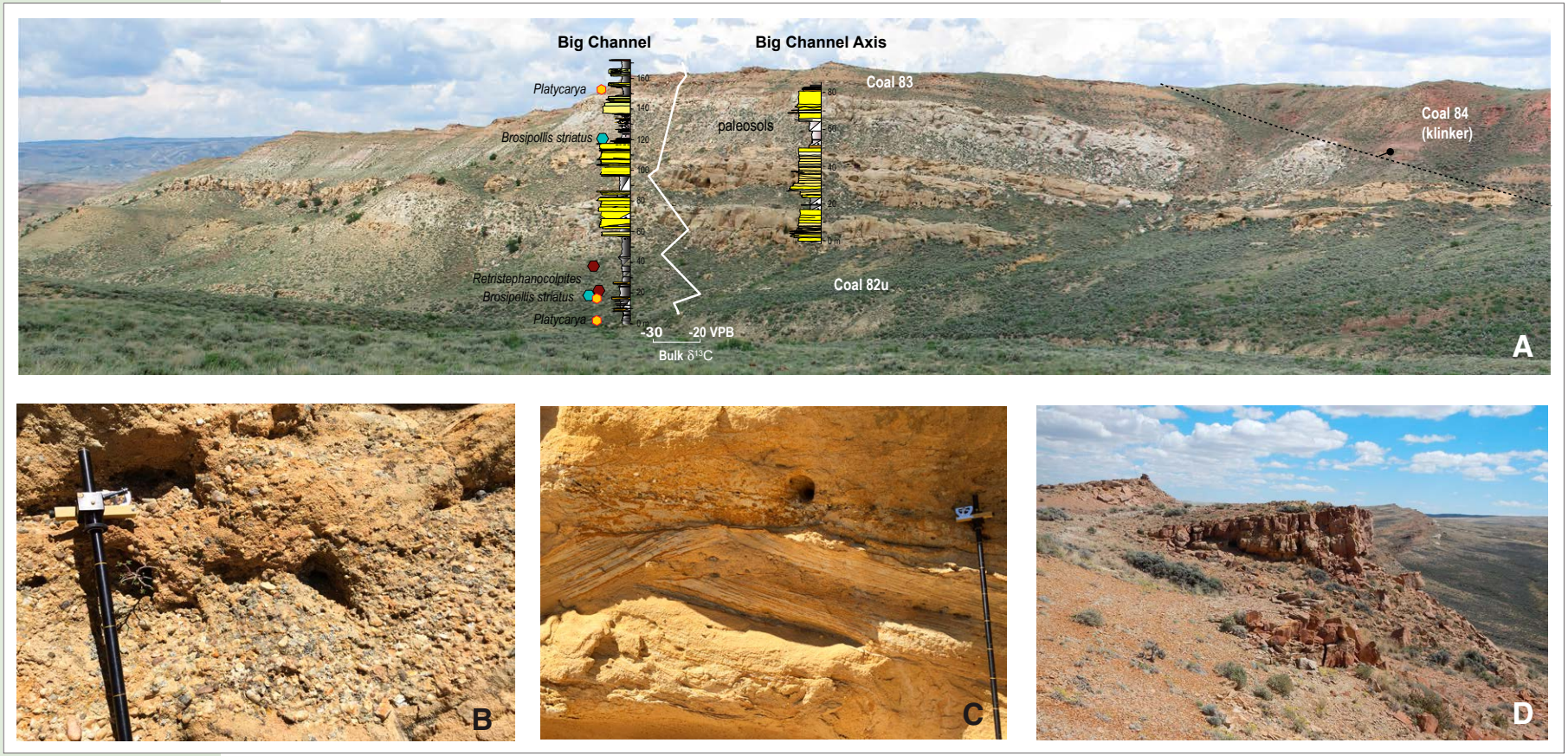

Figure 5. (A) Overview of Big Channel near its axis in Hanna Draw between Coal 82 upper and Coal 83. Big Channel (BC) section is 172 m (565 ft) high. Three amalgamated channel sandstone stories are present, separated by shales, fine-grained siltstones, and sandstones. Between the second and third story, paleosols are common with some orange-to-red mottling. Occurrence of *Platycarya* sp. in the section indicated with yellow hexagon. Offset of the normal fault is ~30 m (100 ft), and it places Coal 84 (red klinker) next to Coal 83 in upper-right corner of picture. (B) Gravel lag composed of chert (likely derived from the Cloverly Formation), Mowry Shale, and some basement clasts is typical for large sandstones in this interval. Clasts are up to 10 cm in this section. (C) Large-scale barforms in Big Channel Axis section in Hanna Draw. (D) Isolated channel (~4 × 20 m) encased in dark and well-developed beds of Coal 83 in the upper part (at 165 m in the Big Channel section), above the amalgamated sandstones within the Paleocene–Eocene boundary. Climbing ripples are common in these sandstones.

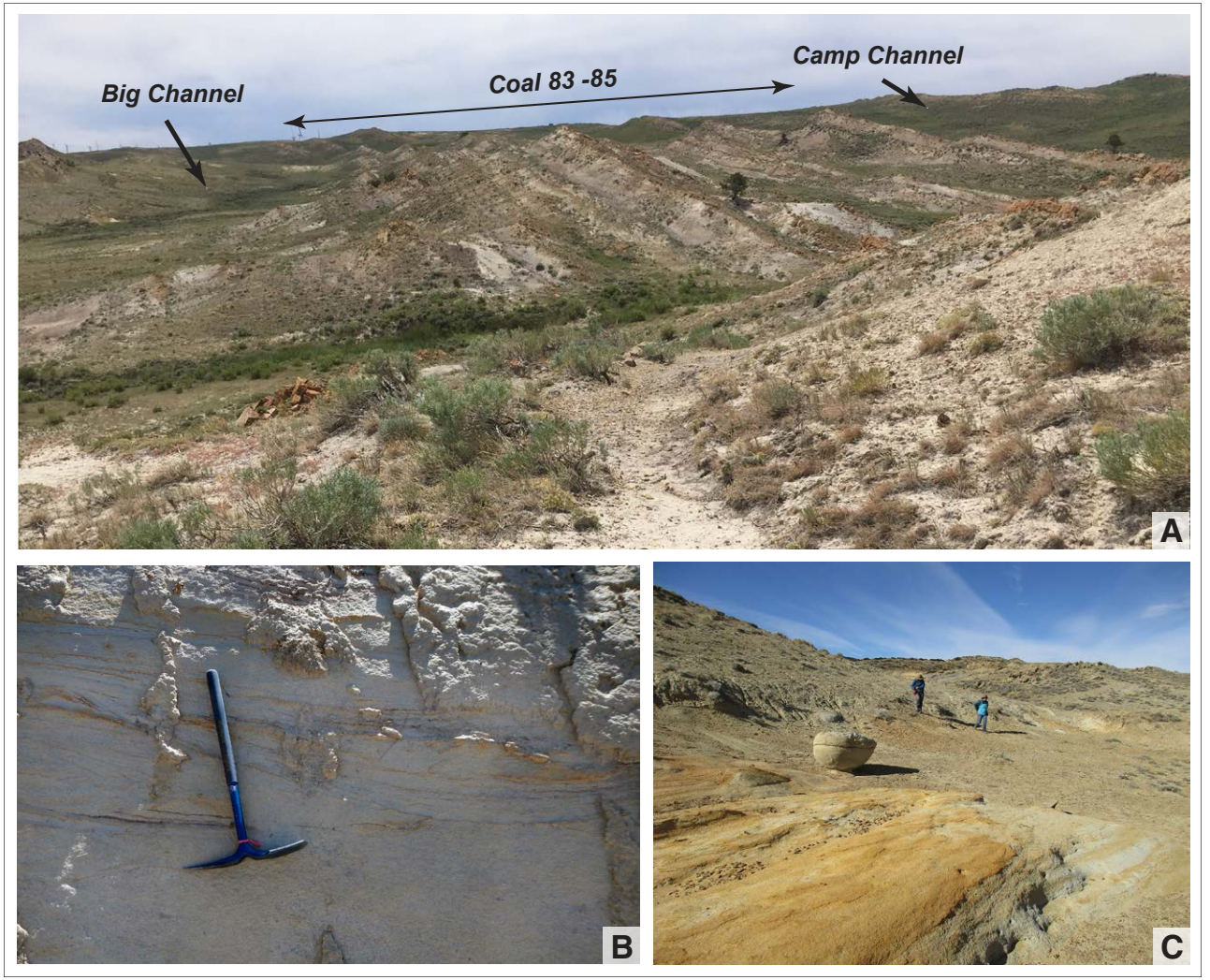

Figure 6. (A) Overview of The Breaks section (TB) (505 m thick), looking south. Note that the soft, easily eroded sandstones of Big Channel and Camp Channel are expressed as recessive intervals. The distinct ridges are formed by meter-scale cycles of carbonaceous shales, to paleosols, and meter-thick sandstones, and often bioturbated ripple beds that are typical for the Coal 83–85 in this area. (B) Example of cross stratification in Big Channel in TB (exposed in a small gulley) and local cobble lags (up to 6 cm). (C) Outcrops of Camp Channel in TB. Large (1.5 × 1 m) concretions occur in the abundantly soft-sediment–deformed, cross-bedded sandstone.

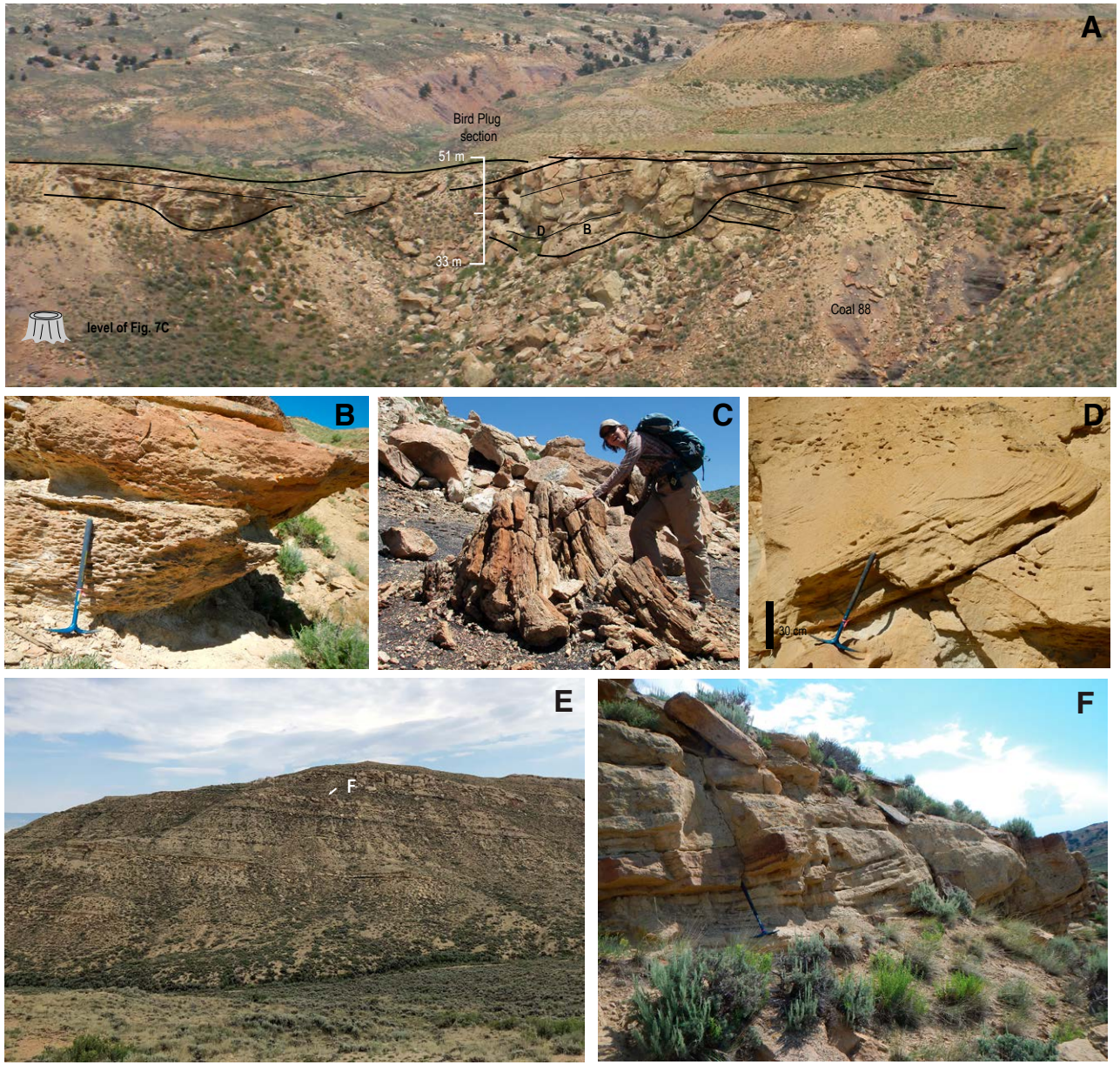

Figure 7. (A) Sandstones at Bird Plug (Coal 88–Coal 88b), looking northeast. Note opposing dips on surface at right flank of main sand body. (B) Climbing ripples in first storey of sandstone. (C) *Metasequoia* tree trunk. (D) Large-scale over-steepened forests. (E) Overview of shallow deltaic to lacustrine shore-face sandstones within Coal 81–82. Arrow points to location of Figure 7. (F) Tangential foresets of ~2.5 m (ft) high interpreted as lacustrine delta.

Comparison of major channel complexes in Hanna Draw

A. Measured Sections

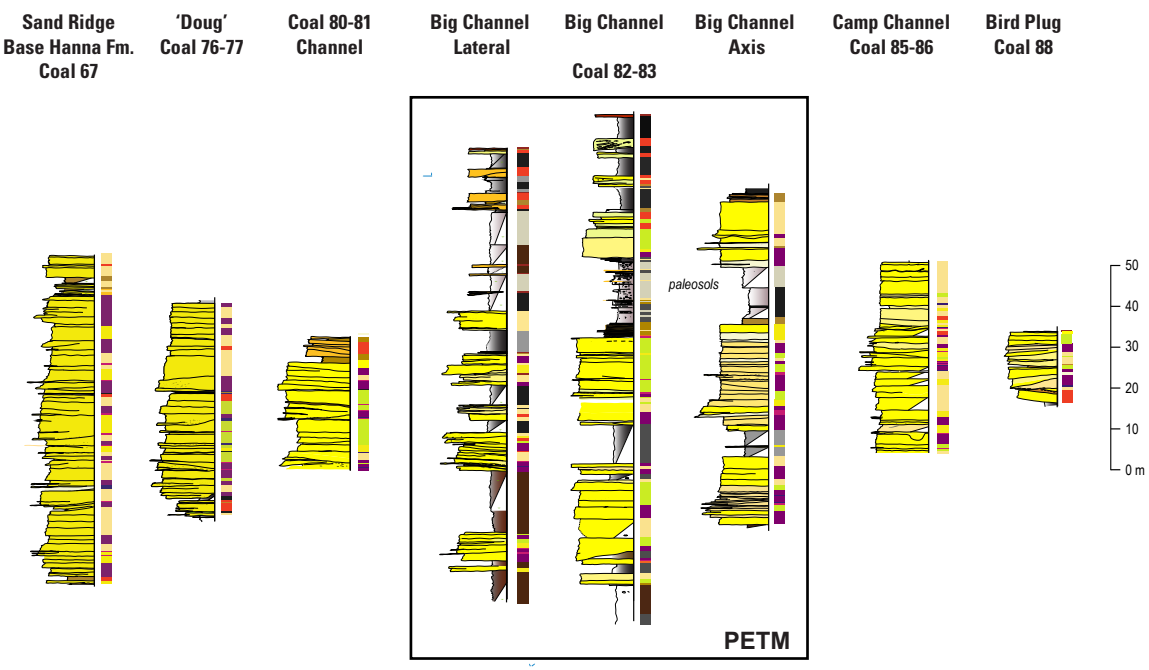

B. Facies distributions and channel dimensions

Relative facies distributions within sandstones

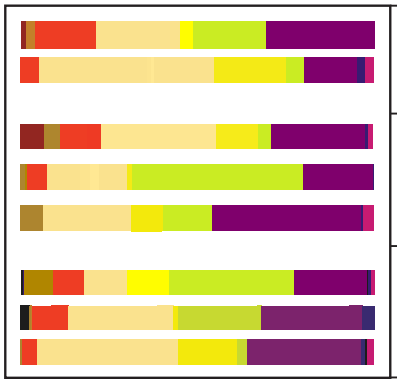

	complex thickness (m)	complex width (m)	maximum clast size (cm)	internal channel thickness (m)	internal channel width (m)
Bird Plug *	17	80	mudclasts	8-15	80
Camp Channel	46	~1500	8	7	175
BCL (PETM)	(9,9,5)	n.m.	1-2	3.7	83
Big Channel (PETM)	(20, 20, 11)	800 - >3000?	6	6.9	155
Big Channel Axis (PETM)	(20, 20, 11)		10	(8-10)	155
Channel above Coal 80	26	1750	4	8	n.m.
Doug	48	2500	6	9	n.m.
Sand Ridge (Base Th)	82	> 10km?	> >?	10 - 12	n.m.

n.m. = not measured

Generalized lithofacies key:

- wave rippled sandstone
- heterolithic sandstone or siltstone
- ripple or climbing ripple sandstone (often bioturbated)
- structureless or soft-sediment deformed sandstone
- trough cross stratification
- planar tabular and climbing dune cross stratification
- low-angle stratification
- mud clast lag
- pebble lag
- brown shale
- gray shale
- mottled paleosol
- dark gray carbonaceous shale

Figure 8. Comparison of major channel complexes in Hanna Draw. Large channel complexes are not uncommon throughout the Hanna Formation. (A) The base of the Hanna Formation (at Sand Ridge) is thickest, most amalgamated, and shows an abundance of pebble and cobble lags and barforms. Total complex thickness decreases toward the Paleocene–Eocene Thermal Maximum (PETM) (see also Fig. 4). The PETM section comprises three large channel complexes at the axis in Hanna Draw; these complexes split up laterally toward Big Channel Lateral (BCL) and amalgamate near The Breaks (TB) (not shown in this figure). Early Eocene Camp Channel is more amalgamated and shows abundant soft-sediment deformation. Bird Plug (asterisk) is either a very distal expression of channel complex or a delta into a shallow lake. Paleosols are present between channel complexes 2 and 3 in the Big Channel interval. Figure 1B compares facies distributions for large fluvial sandstones from the bottom to top of the section. Structureless sandstone and ripple to climbing rippled sandstone percentages increase for each sand body upward in section, while pebble lags and barforms decrease (mud clast lags increase). There appear to be two trends of decrease in channel sizes upward—one below Big Channel and one above. Big Channel has somewhat coarser clasts and more tractional structures than the channel below. Channels within Big Channel (internal channel dimensions) remain quite constant throughout the section.

Figure 9. (A) Coarse angular gravel lag with abundant Mowry Shale near Beer Mug Vista (BMV). (B) Overview of the stratigraphy near BMV. Changes in dip from bottom to top suggest progressive deformation during deposition. (C) Red paleosols in the lower half of BMV.

The lower part of BMV section is characterized by orange-to-red mottled paleosols, suggesting well-drained rather than swampy conditions near the basin margin (Fig. 9C). As observed in the other sections, above Coal 87, carbonaceous shales and carbonate concretions increase and suggest regional lake and swamp expansion (Fig. 4).

Paludal and Floodplain Deposits

Coal and carbonaceous shale intervals occur in all sections and vary from 5 to 40 m (15–130 ft) thick and are laterally correlative over kilometers. Carbonaceous shales can range from dark gray to black and dark brown and commonly contain plant remains, gypsum crystals (selenite), and siderite concretions. Highest-grade coals are black, vitreous, and crumbly when encountered in outcrop. Light- to dark-gray immature paleosols have commonly developed in carbonaceous shales. Carbonaceous shales and siltstones alternate with light-gray, carbonate-cemented, fine-grained sandstone beds that are capped with oscillation ripples or vertical burrows and bedding-parallel feeding traces (*Planolites*; Fig. 10). Small vertical burrows up to 1 cm (0.5 in) are also common in rippled, fine-grained sandstone beds.

Presence of extensive coal and carbonaceous shale intervals indicate permanently inundated floodplains, ponds, or swamps with ample vegetation, which is corroborated by the abundance of *Metasequoia* tree trunks and foliar remains of *Averrhoites affinis, Equisetum* sp., *Zingiberopsis isonervosa,* and various ferns. Crumbly, light- to dark-gray, structureless, sandy and silty shales and siltstones with slickensides, mottling, and root casts indicate immature pedogenesis and changes between inundated and less wet conditions (Glass and Roberts, 1984). The orange- to red-mottled paleosols found near the basin margin (BMV) and in the fluvial sandstone interval at BC indicate low groundwater levels and oxidizing conditions that are generally related to better soil drainage (Kraus et al., 2013). However, these better drained soils are rare within the study area.

Crayfish traces, ranging from 3 to 8 cm in diameter and up to 1 m deep, occur in light-gray shale to fine-grained sandstones with immature paleosols between Coal 83 and Coal 85 in The Breaks (Fig. 10). Crayfish trace fossils have only been found in The Breaks and are typical for areas of fluctuating water tables and seasonality in groundwater levels (Hasiotis and Honey, 2000).

Lacustrine Sandstones and Shales

Deepest lacustrine deposits in the study area consist of chocolate- to dark-brown- to gray shales that often contain fish fragments such as scales and bones, insect wings, gastropods, and bivalves. These deposits alternate with siltstones, carbonaceous shales, and coals of paludal origin, and the boundary between shallow lake, swamp, and permanently inundated floodplain is not always clear. Mollusk preservation appears more prevalent in predominantly lacustrine intervals as water level deepened, and often fish fragments are found nearby.

A millimeter-scale laminated, fine-grained limestone bed with abundant gastropods of which the taxa are unidentifiable and show only few signs of transport occurs as a characteristic 8–15 cm bed in Coal 87, both in Hanna Draw and The Breaks. Limestone beds like this typically indicate freshwater conditions and are common in shallow ponds or littoral lacustrine environments with vegetation (Carroll and Bohacs, 1999; Alonso-Zarza, 2003; Bowen et al., 2008). The limited transport damage suggests that this bed was not a true coquina but deposited in a low-energy littoral lacustrine environment. Carbonate cementation and concretions occur throughout the section but

Figure 10. (A) Upper part (~170 m) of Big Channel Lateral (BCL) exhibits abundant scours, trough cross bedding, and climbing ripples. (B) Soft-sediment–deformed ripple bed interpreted as distal splay (Coal 87). (C) Thin-bedded coarsening-up sequence with wave ripples (between Coal 81 and Coal 82). (D) Oscillation ripples (just above Coal 77). (E) Bedding-parallel gypsum beds in Coal 90; pencil for scale. (F) *Planolites* burrows often found in ripple beds just below carbonaceous shale and coal intervals (Coal 81; pick axe handle is ~3 cm in diameter). (G) Carbonate concretion on top of ripple bed in The Breaks. Davis (2006) has interpreted these limestone beds as stromatolites; however, no distinct internal laminations are observed, and no additional isotopic analysis was done. (H) Crayfish burrows in The Breaks.

significantly increase above Coal 87, suggesting that the basin became more enclosed. Some of the carbonate-cemented beds have been described as stromatolites in earlier work (Fig. 10; Davis, 2006).

Upward coarsening and thickening packages of light-gray, fine-grained, rippled sandstones suggest lacustrine shore-face environments (Fig. 10C). These are particularly prevalent in Coal 81–82, but also Coal 77–78. Thin, parallel-bedded sandstones with isolated and stacked ripples are encased within shales and occur in both The Breaks and Hanna Draw. Swaley cross bedding indicating wave action is not common but does occur in The Breaks and near Coal 76 in Hanna Draw. Siltstones and shales associated with these coarsening-up packages are remarkably void of organic material, which might indicate higher depositional energy near the lake margin.

Most common between Coal 81 and Coal 82 are extensive packages of unidirectional, up to 2- and 3-m-high foresets. Internal grain sizes fine toward foreset bottoms, and inversely graded internal laminae suggest that these are small deltas or mouth bars, like ones found in deposits of similar age in the nearby North Park–Middle Park Basin (Flores, 1990; Dechesne et al., 2013).

Noteworthy in Coal 90 are thin beds (1 cm thick) of gypsum within dark-brown to gray shales alternating with siltstones containing fish fragments (Fig. 10). The gypsum layers are bedding parallel and interpreted as primary deposit. They also corroborate more restricted conditions in this part of the section as indicated by the increase in carbonate concretions and cement.

Paleobotany

At Hanna Draw, plant localities below the Big Channel Complex are dominated by *Metasequoia occidentalis* (Newberry) Chaney (Cupressaceae), *Platanites raynoldsii* (Newberry) Manchester (Platanaceae), *Trochodendroides genetrix* (Newberry) Manchester (Cercidiphyllaceae), *Zizyphoides flabela* (Newberry) Crane, Manchester and Dilcher (Trochodendraceae), *Archeampelos acerifolia* (Newberry) Mciver and Basinger (Cercidiphyllaceae), and *Macginitiea gracilis* (Lesquereux) Wolfe and Wehr (Platanaceae), all of which are abundant throughout the Rocky Mountain basins during the early Paleogene, particularly in riparian environments. Taxa that are restricted to the Paleocene, including *Cyclocarya brownii* Manchester and Dilcher and *Cornus swingii* Manchester, Xiang, Kodrul, and Akhmentiev confirm that these sites predate the Paleocene–Eocene boundary. The first definitively Eocene macrofossils in the Hanna Draw section are *Platycarya* sp. leaves and catkins, which occur at the 707 and 728 m level in the Hanna Draw Section (Coal 84 of Dobbin et al., 1929; localities EC1501 and EC1506 and 1509, respectively). The first appearances of *Lygodium kaulfussi* (locality EC1509) and *Salvinia preauriculata* (locality EC1502) occur close by, respectively at 45 and 60 m higher in the section (Fig. 4; Supplement S1 [footnote 1]).

Early to middle Paleocene plant fossils in The Breaks were described and censused in Dunn (2003). Leaflets of Wing and Currano's (2013) "Dicot sp. WW004," a Bighorn Basin morphospecies that is common in the PETM interval and does not occur in any other part of the section, were recovered at the 120 m level in The Breaks section. *Platycarya* sp. and *Cnemidaria magna* leaves first occur laterally equivalent to 318 m in The Breaks section (150 m [500 ft]) above the top of Big Channel), and *Lygodium kaulfussi* occurs at ~333 m, laterally projected into The Breaks section (165 m [540 ft] above Big Channel, Figs. 11A–11C). Leaves and pollen cones of *Alnus* sp. were recovered below the first appearance of *Platycarya* sp., at site ECHB 1609. Because *Alnus* leaves are restricted to the Eocene in the Greater Green River and Bighorn Basins (Wing, 1998; Wilf, 2000) and only occur above the first occurrence of *Platycarya* sp. in the Hanna Draw section, this stratigraphic level can also be classified as Eocene.

Palynologic occurrences of *Platycarya platycaryoides* (Fig. 11D) precede the leaf fossil occurrences in both The Breaks and Hanna Draw sections and help more broadly constrain the proposed PETM interval. *Platycarya* pollen, typical for the recovery phase of the carbon isotope excursion (CIE) in the Bighorn (Wing et al., 2005) and Powder River Basins (Wing et al., 2003), first occurs 54.5 m (180 ft) below the base of the first channel of the Big Channel Complex (sample 18BC-2.57 m) and again 32.6 m (106 ft) below the base of the Big Channel Complex (sample 18BC-24.4 m). It is then absent in all subsequent samples until it appears again in Coal 83, 39 m (128 ft) above the uppermost channel story of the BCC (sample 16BCr-155). A similar pattern is found in The Breaks where *Platycarya platycaryoides* first occurs 24 m (78 ft) below the base of the Big Channel sand (106 m in the measured section) and appears again in the mostly covered interval near the top or within the Big Channel at the 176 m level. *Platycarya platycaryoides* pollen is then more commonly found in samples beginning at the 206 m level in The Breaks section. Our first occurrence datum of *Platycarya platycaryoides* in The Breaks occurs lower in the section than previously reported (Lillegraven et al., 2004; Pew, 2014).

In the Big Channel Lateral (BCL) section, we were unable to detect the first pulse of *Platycarya* pollen below the Big Channel bed. Instead, it first appears 19 m (62 ft) above the Big Channel Complex, 170 m high in the local section (sample HB-RD17-007). At this sample location, it occurs abundantly as it does in The Breaks and Hanna Draw sections above the Big Channel Complexes at each of these sites.

In the Hanna Draw section, another key Eocene pollen taxon, *Intratriporopollenites* cf. *instructus* (Fig.11E), first appears with *Playtcarya platycaryoides* in samples 18BC-2.57m and 18BC-24.4m. *Brosipollis striatus* (Fig. 11F) occurs in several samples between 24.4 m and 129 m, and *Retristephanocolpites* sp. (Fig. 11G) occurs fleetingly at 29.6 and 36.1 m. These two taxa are known to occur only during the PETM in the Gulf Coast and Rocky Mountain region (Harrington et al., 2015). The fern spore *Granulatisporites* sp. is another Eocene indicator in the Gulf Coast (Harrington, 2003b) that also occurs in the Hanna Draw section at 24.4 m (Fig. 11H). Palynological samples between 50 and 123 m had generally poor palynomorph preservation. Following this interval, two new Eocene taxa from the Gulf Coast appear at 123 m in the section, *Corsinipollenites psilatus* (Fig. 11I) and *Interpollis microsupplingensis.*

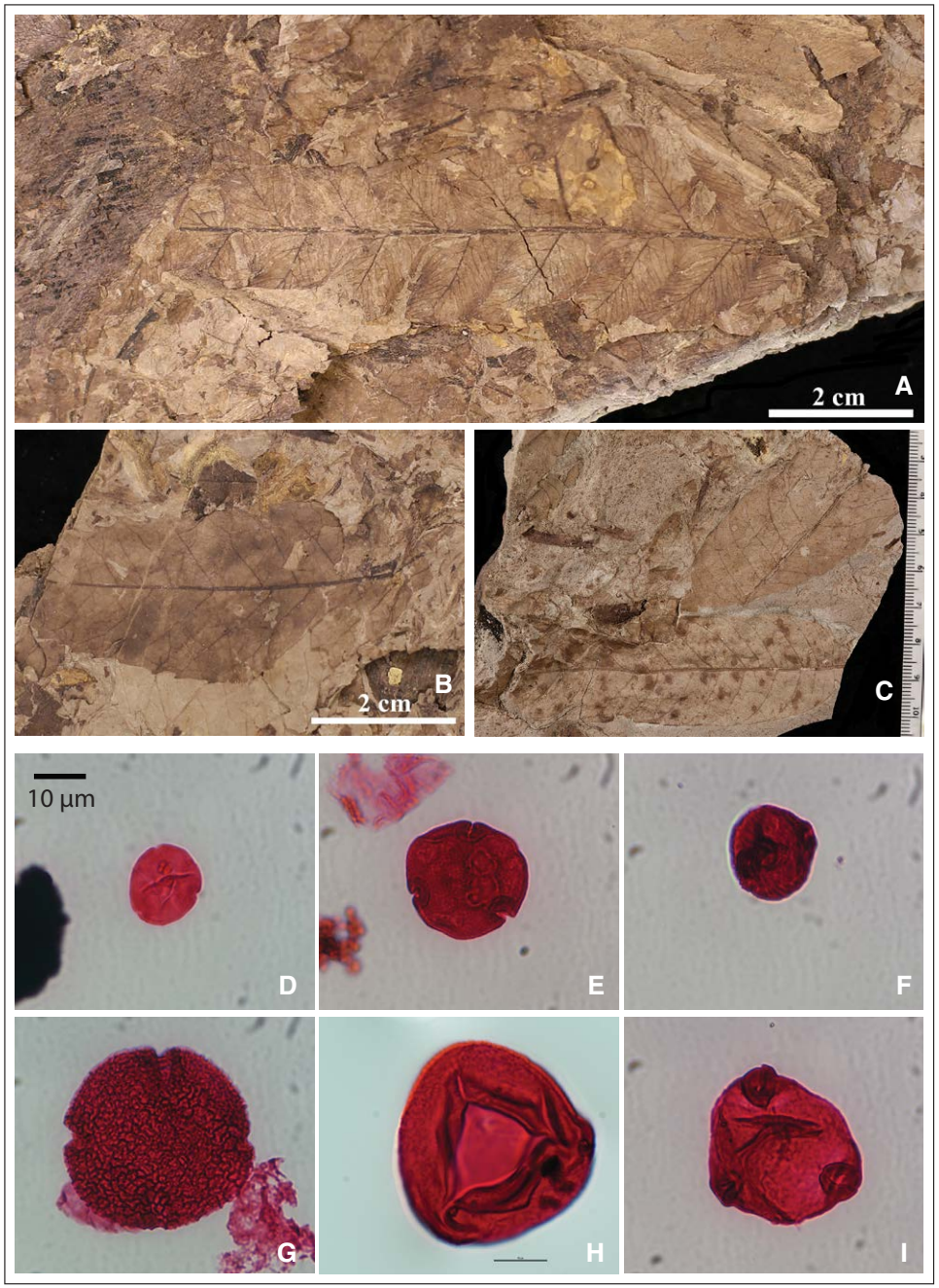

Figure 11. Pictures of Eocene indicator taxa: (A) *Cnemidaria magna* leaf imprint (locality EC 1611); (B) *Platycarya* sp. leaf imprint (locality EC 1611); (C) Dicot sp. WW004 from locality ECHB1807. This leaf morphospecies is common in the Paleocene–Eocene Thermal Maximum (PETM) of the Bighorn Basin, northwest Wyoming (Wing and Currano, 2013). (D) *Platycarya platycaryoides* (locality 18BC-2.57); (E) *Intratriporopollenites* cf. *instructus* (locality 18BC-2.57); (F) *Brosipollis striatus* (locality 18BC-29.6); (G) *Retristephanocolpites* sp. (locality 18BC-29.6); (H) *Granulatisporites* sp. (locality 18BC-24.4); (I) *Corsinipollis psilatus* (BC16-123m). Photographs A–C by E. Currano; photographs D–H by R. Dunn.

Continental Mollusks

There are over 200 Paleogene continental molluscan localities in the Hanna Basin, of which the hydroboids, viviparids, and sphaeriids could be used to demarcate the Paleocene–Eocene boundary. Mollusk occurrence in our section also indicates more lacustrine than fluvial or paludal conditions (Fig. 5; Supplement S1 [footnote 1]). Unfortunately, preservation varies between localities, and species are not always easy to identify because the continental shells are (1) simple in form, (2) considered variable (in time, space, and environment), (3) frequently deformed, and (4) preserved without quality shell material. On top of this, some of the localities are in coarse-grained sandstone granule conglomerate interpreted as local lag accumulations (e.g., L7043 in The Breaks, 26 m above the top of Big Channel).

The hydrobioid *Micropygus minutulus* (Meek and Hayden), which was recognized from the late Tiffanian in the Williston Basin (type occurrence) and the Clarkforkian in central Utah (La Rocque, 1960), occurs in Coal 80 in Hanna Draw (L7306; Supplement S1 [footnote 1]). The younger molluscan assemblage at and below Coal 82 (L7358, just below the PETM; Supplement S1) represents conventional late Paleocene morphologies similar to the Bighorn and Powder River Basins. However, compared to the diverse assemblages there, species richness is limited in the Hanna Basin (Hartman and Roth, 1997, 1998). In Coal 82 in The Breaks, one small incomplete pleurocerid specimen was found with axial sculpture most commonly present on species of *Elimia* (L7528; Coal 82, TB; Supplement S1); however, exact age designation remains uncertain due to preservation and correlation issues. Wasatchian pleurocerid *Elimia tenera* (Hall) was discovered in Coal 85 in The Breaks (L7524; Supplement S1; see also Fig 12A).

Transported viviparids are not uncommon in the section, such as at L7523 in The Breaks (278 m; Supplement S1 [footnote 1]; at 92 m (300 ft) above the PETM; Fig 12B). Hanna Basin viviparid specimen identifications are most likely to be compared *to Paludotrochus uniangulatus?* (Hall), *Paludotrochus paludinaeformis* (Hall), and *P.* aff. *P. wyomingensis* (Meek) after Hartman (1984), which otherwise have an early Eocene distribution. Although incomplete and/or variously compressed, a few specimens bear traits that indicate assignment to the early Eocene *Paludotrochus paludinaeformis* (L7350, Coal 87, ~245 m above the PETM in Hanna Draw), which is common in lower Eocene lacustrine lithic units elsewhere in Wyoming. T.W. Stanton (1916) identified a questioned occurrence (L3511) of the taxon, along with another early Eocene species, *Physa pleromatis* White, near Coal 90. The reason for absence of other early Eocene continental mollusks needs further study.

Bulk Carbon Isotope Curves

The bulk organic carbon isotope data are plotted on Figure 4. The main $\delta^{13}C_{org}$ signal between Coal 77 and Coal 82 is constant along Hanna Draw and

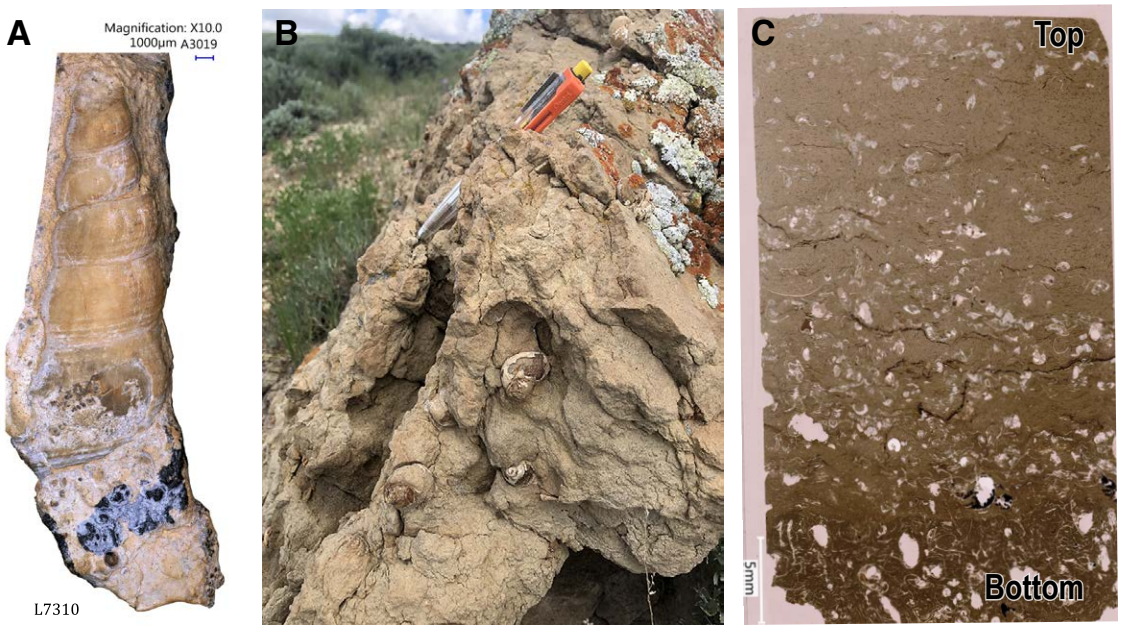

Figure 12. (A) One of the better preserved mollusk specimens of biostratigraphic importance *Elimia tenera?* (Hall), L7310 (Kirschner, 1984, locality 4) from Coal 87, ~750 m north of The Breaks section (Supplement S1 [text footnote 1]). Photograph by J. Hartmann. (B) Transported mollusks at the top of The Breaks (TB) section. (C) Thin section of the gastropod limestone bed in Coal 87. Gastropods show little sign of transport.

ranges from –25.1‰ to –26.6‰ VPDB (Supplement S3 for data and sample coordinates [footnote 1]). A large shift in $\delta^{13}C_{org}$ occurs between the last occurrence of Paleocene plants and the first appearance of earliest Eocene plants in the interval between Coal 82 upper and Coal 83. Both the most positive (–23.5‰) and most negative (–30.8‰) values occur in this part of the section, and likely reflect the carbon isotope excursion (CIE) globally found at the PETM. Above Coal 83, isotope values range from –25‰ to –28.3‰.

Bulk $\delta^{13}C_{org}$ isotopes in The Breaks vary from –25.2‰ to –27.8‰ and do not reveal a clear CIE. Exposure is poor in the Big Channel interval of The Breaks, precluding isotope samples from this part of the section. In The Breaks, the $\delta^{13}C_{org}$ isotope signal appears to correspond with the pattern of a series of coarsening-up sequences, containing ripple beds and immature paleosols, often capped with thin gravel lags. The gravel lags, which often include reworked siderite clasts (such as in the Carbon Basin; Loope and Secord, 2017) and 2–5 cm angular clasts of organic, carbon-rich Cretaceous Mowry Shale (or other Cretaceous shales) derived from the emerging Seminoe Mountains and Freezeout Mountains.

Zircon Ages

Five of the very fine-grained mudstones samples suspected to be tonsteins were run for ID-TIMS U-Pb zircon dating. One of the five samples, RD0814-36, collected in Coal 88 in The Breaks, contains zircons that are ca. 54 Ma (Supplement S2a, Table S2-1 [footnote 1]). However, this sample also contained numerous euhedral zircon grains that are much older than the expected volcanic age (Supplement S2a, Figs. S2-1, S2-2, and S2-3). Nine zircons yielded dates of ca. 55 Ma (Supplement S2a; Fig. S2-4a), with a spread in $^{206}Pb/^{238}U$ dates from 57.0 to 53.8 Ma. The best estimate on the age of deposition comes from the Concordia Age (Ludwig, 1998) from the four youngest, overlapping, concordant single-grain analyses, 54.42 ± 0.27 Ma (95% confidence including decay constant errors; Supplement S2a, Fig. S2-4b).

Surprisingly, these young grains are from the euhedral, nearly equant population rather than the elongate grains that exhibit more characteristic ash-fall morphologies. The youngest grain dated from the "ash-fall" morphology (euhedral, elongate grains) sub-population in this sample is 56.0 ± 0.7 Ma (Table S2-1, Supplement S2a [footnote 1]). The five slightly older zircons, including two with apparent ash-fall morphologies, have $^{206}Pb/^{238}U$ dates that range from to 57.1 ± 1–55.2 ± 0.3 Ma. They are interpreted to reflect either pre-eruptive, antecrystic zircons from the magma chamber or slightly older volcanic grains from earlier events that were entrained during the latest eruption. Single-grain analyses from the other four samples are all older than 74 Ma (Supplement S2a), despite displaying euhedral morphologies, and are interpreted to be detrital.

To address the largely inherited component of zircon in the samples and to screen for more zircons that may represent the age of deposition of the strata, four of the mudstones plus four additional, fine-grained sandstone samples were analyzed by LA-ICPMS (Supplement S2a and S2b [footnote 1]). In general, the sandstone samples have very low zircon yields (fewer than 100 grains in all samples and generally less than 40) and few concordant grains that are Cenozoic in age. Sample RD0814-35, which is from nearly the same stratigraphic horizon in The Breaks as the sample that provided the ca. 54 Ma concordant zircon (RD0814-36), had a single young grain at ca. 54 Ma (Supplement S2b), which is the best limit on deposition age from the zircon data. Based on the zircon age distributions, it appears that there are very few if any ash-fall zircons, and it is possible that the sampled units are not directly derived from volcanic ash but rather fine-grained siliciclastic to clay-rich sediments in very low-energy environments, possibly fluvial floodplain deposits.

DISCUSSION

PETM

Diagnostic late Paleocene and early Eocene paleobotanical remains, incorporated with geochemistry, and stratigraphic correlations, allow us to more precisely place the PETM within the Hanna Formation. Occurrence of late Paleocene plants in Coal 82 and the presence of Eocene indicator taxa above this level best constrains the Paleocene–Eocene boundary in our data set both in Hanna Draw and The Breaks (Fig. 4). *Platycarya* is thought to be an immigrant taxon that first arrived in North America during the earliest Eocene from Europe where it occurs in the latest Paleocene (e.g., Jolley, 1997). As such, *Platycarya* pollen has historically been used as a marker taxon in defining early Eocene strata in the Western Interior (Nichols and Ott, 1978). Further refinements of when *Platycarya* pollen first appears in relation to the PETM have shown it occurs in the recovery phase of the CIE in the Bighorn and Powder River Basins (Wing et al., 2003, 2005) and during pre-CIE warming in the North Sea (Eldrett et al., 2014) and Gulf Coast (Sluijs et al., 2014). The first appearance of *Platycarya platycaryoides* in the Hanna Basin below the CIE, consistent with the higher-resolution records of the Gulf Coast and North Sea marine cores, confirms that *Platycarya* first occurs in the latest Paleocene in North America as well. The slightly later occurrence of *Brosipollis striatus* and *Retristephanocolpites* sp. ~20 m higher than the first appearance datum (FAD) of *Platycarya platycaryoides* in the Hanna Draw section, is consistent with PETM occurrences of these taxa in the Gulf Coast and in other basins in Wyoming (Harrington et al., 2015). In total, in the Hanna Draw section where the palynology is best constrained to date, we find the first appearances of six taxa known from the PETM or earliest Eocene between 24.4 m (30 m below the first sand channel) and 123 m high in the section. Additionally, the presence of a Bighorn Basin PETM leaf morphotype within the Big Channel sequence in The Breaks provides additional evidence that the PETM event is captured at this stratigraphic level in multiple places in the basin.

Our geochemical data were collected over the entire studied interval to locate the CIE that marks the PETM. In the Hanna Draw section, bulk $\delta^{13}C_{org}$

isotopes start deviating from a near-constant background value of about –26‰ (VPDB) below Coal 82, to values both more negative (minimum –30.8‰ VPDB) and more positive (maximum –23.5‰ VPDB) between Coal 82 and 83 (see Fig. 5), concurring with the PETM from our paleobotanical data. Just above Big Channel in Coal 83, the bulk carbon isotope signal stabilizes to more-or-less pre-CIE background values (Fig. 5); however, the signal remains slightly more erratic than before the CIE in both Hanna Draw and The Breaks (also Higgins, 2012).

Higgins (2012) originally identified an area with erratic $\delta^{13}C_{org}$ values within Coal 84 and 85 as the CIE in The Breaks; however, our new isotope data, stratigraphic correlations, and paleobotanical data indicate that the CIE must occur lower than originally placed. Identifying a CIE with bulk $\delta^{13}C_{org}$ in The Breaks has proven harder than in Hanna Draw because Big Channel is poorly exposed, and our sampling density has not been tight enough (Fig. 4). Contamination with modern soil or influx of allochthonous carbon due to weathering and erosion of older carbonaceous material in the surrounding drainage areas could be additional explanations for erratic bulk $\delta^{13}C_{org}$ signals (Baczynski et al., 2016; Lyons et al., 2017).

Continental mollusks of the Hanna Formation are less diverse than in neighboring basins, and poor preservation of specimens limits us from using this data set to better constrain the PETM and early Eocene stratigraphy. However, the mollusk data set shows a change around the PETM (localities L7358, L7528, L7043, and L7523) and supports previous work on ostracods and mollusks (Glass, 1980; see Kirschner, 1984, p. 59). Preserved morphologies of caenogastropods (Viviparidae, Pleuroceridae, and Hydrobiidae), veneroids (Sphaeriidae), and unionioids (Unionidae) are consistent with taxa for a late Paleocene age in localities below Big Channel. Likewise, sparse specimens from localities above Big Channel indicate lower Eocene from different taxa in same families. A significant loss of taxa (caenogastropods, in particular), occurs across the Paleocene–Eocene boundary, but unlike the Bighorn and Powder River Basins, the Hanna Basin does not acquire any pulmonate taxa (Hartman and Roth, 1998).

In contrast with the significant changes in sedimentary facies documented in other basins that are generally more arid in setting (Foreman et al., 2012; Foreman 2014; Colombera et al., 2017), it is remarkable that facies distributions and channel dimensions within the PETM interval in the Hanna Basin are not as different between major channel complexes (Fig. 8). Comparison of facies within each of the large sandstone complexes shows a general decrease in the occurrence of large barforms and lag deposits upward in our studied section, plus an increase in soft sediment deformation, ripple, and climbing rippled sandstones. Big Channel does interrupt this trend and occurs at the identified PETM, between Coal 82upper and 83. Lags and large barforms are more abundant than in the channels directly below or above. Also, three channel intervals occur within the here-identified CIE, rather than one large amalgamated sandstone complex. The second and third stories are separated by an interval with abundant orange-to-red mottled paleosols, which is rare within the generally paludal deposits of the Hanna Basin.

Paleogeography

Regional compilations of paleoriver systems by Galloway et al. (2011), Smith et al. (2014b), and Sharman et al. (2017) indicate the presence of west- to east-directed rivers through the Hanna Basin and possible connections with a larger (California) River during the Paleocene. Paleoflow directions within the study area indicate a dominance of east- and northeast-directed flow, which corroborates this flow pattern and suggests basin-axial flow (Figs. 4 and 5; Ryan, 1977; Wroblewski, 2002).

Progressive basin isolation by the emergence of surrounding uplifts such as the Rawlins uplift, the Freezeout Mountains, Laramie Range, Medicine Bow, and Sierra Madre, coincides with the relative upward increase in ponded facies above Coal 87, and southward transport directions in TB and BMV indicate very limited basin-axial transport and increased influx from the northern basin margin. (Fig. 13; Blackstone, 1993; LeFebre, 1988; Perry and Flores, 1997; Wroblewski, 2002; Flores, 2003; Loope and Secord, 2017). Emerging uplifts caused drainage reorganization and possibly climatic rain shadows that changed water balance and sedimentation patterns in the basin. The gastropod limestone bed in Coal 87 and the evaporites in Coal 90 indicate more restricted conditions often seen at the late-stage fill of an overfilled lake basin and the transition into a more restricted basin fill (Carroll and Bohacs, 1999; Alonso-Zarza, 2003). The evaporites indicate that evaporation became greater than freshwater input, suggesting internal drainage and possibly the onset of drainage reversal from east- to west-directed rivers during the Eocene.

The repetitive pattern of laterally extensive sandstones that are similar in appearance (Figs. 3 and 4) throughout the entire Hanna Formation beyond the PETM, invites speculation on the origin of this cyclicity. Factors such as topography building, channel migration, and avulsions that are internal to a depositional system have been identified to cause an autocyclic succession of channel and floodplain deposits in the underlying Ferris Formation near the study area, however, at a smaller scale (Hajek et al., 2012). Aswasereelert et al. (2013), Smith et al. (2014b), and Noorbergen et al. (2017) link pronounced cyclicity in the Paleocene and Eocene sediments in the Bridger and Powder River Basins to climate and orbital signals such as 100 k.y. short eccentricity. Alternatively, the fluvial sandstone intervals at Big Channel and Camp Channel could reflect sedimentary responses to climate effects of early Eocene hyperthermals, because Big Channel coincides with the PETM based on our data. If the ca. 54.4 Ma zircon age from Coal 88 is indeed detrital, the timing of deposition of Camp Channel could coincide with the next large Eocene hyperthermal, ETM2 at ca. 54 Ma (Westerhold et al., 2007).

Provenance assessment derived from our zircon analysis does not reflect the ages of local Precambrian basement. The Hanna Basin is located near the junction of the >2.5 Ga Wyoming craton, 2.0–1.8 Ga Mojave province, and 1.8–1.7 Ga Yavapai province (e.g., Amato et al., 2008), a Proterozoic suture zone termed the Cheyenne belt (e.g., Duebendorfer et al., 2006). Since the majority of zircon grains analyzed appear to be inherited and/or detrital in nature, we created a composite plot of all samples with greater than ten individual

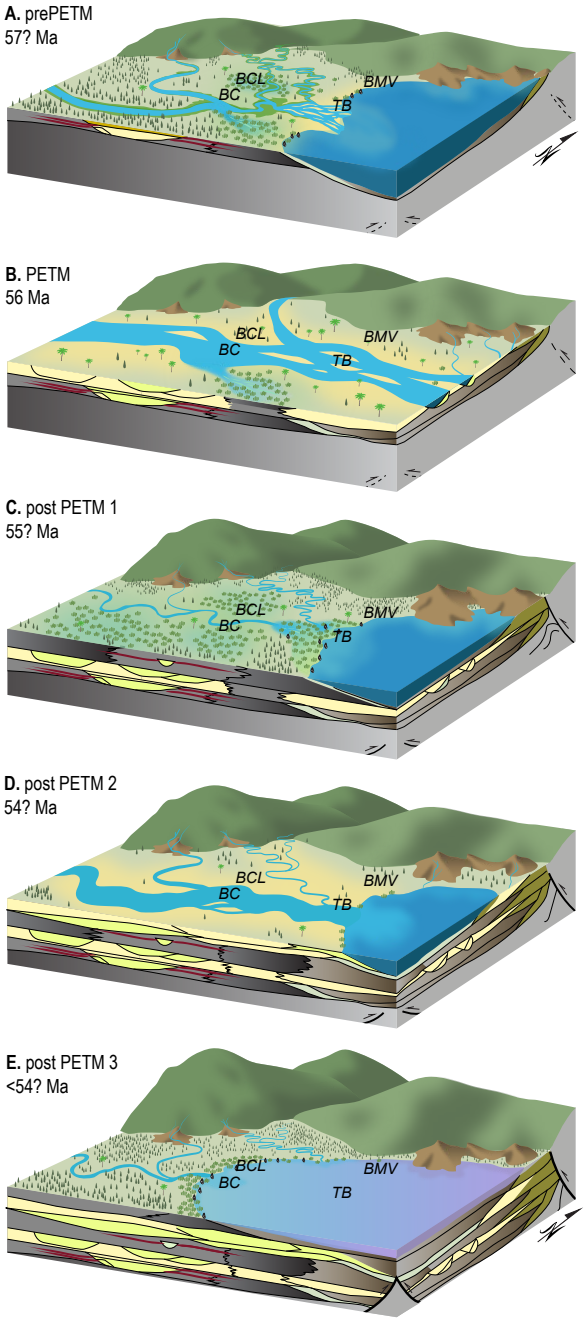

Figure 13. Paleogeography of the Hanna Formation in the study area showing pre-, during- Paleocene–Eocene Thermal Maximum (PETM), and post-PETM increased isolation of the Hanna Basin, and varying sediment input. View looking north toward the Freezeout Mountains. Vegetation is schematic, and approximate section locations are indicated (BC—Big Channel; BMV—Beer Mug Vista; TB—The Breaks; and BCL—Big Channel Lateral). (A) Pre-PETM (Coal 77–Coal 82): uplifts surrounding the basin were not as pronounced, and a connection to the west with the greater Green River Basin likely still existed. To the south, the Medicine Bow Mountains were likely already uplifted (Peyton and Carrapa, 2013). An outlet for the main axial river system is uncertain at this time, and lacustrine incursions are common before the PETM as well. (B) During the PETM (Coal 82 upper–Coal 83, 56 Ma), fluvial systems expanded in the area, and a main axial river system dominated sedimentation across the entire study area. It is uncertain how much connection remained between the Greater Green River Basin and the Hanna Basin during the PETM. Data from Ryan (1977) suggest that most material in the Hanna Formation was locally derived. (C) Post-PETM (Coal 84–Coal 85): The interval of Coal 83–85 is dominated by carbonaceous shales and abundant plant remains, typical paludal deposits, with some lacustrine incursions. The basin became more isolated due to continued rise of surrounding uplifts and possibly reorganized drainage systems. (D) Camp Channel is the last big pulse of sediment deposited by the dominant axial river system in this area. (E) Lacustrine deposition became more dominant. Increased carbonate cementation and thin gypsum evaporite beds suggest that the basin lacked large amounts of freshwater input and was more enclosed (evaporative conditions are indicated by slight pink coloring of the lake).

grains analyzed, a total of 156 analyses. The composite detrital zircon Hanna Basin sample has a major peak at ca. 1.7 Ga, which is typical of basement terranes to the south, but has only few grains older than 1.8 Ga (Supplement S2a, Fig. S2-5 [footnote 1]). Other detrital zircon age populations present in the composite sample include ca. 650–500 Ma (peri-Gondwanan terranes) and ca. 480–270 Ma (Appalachian terranes) and a minor ca. 1100–900 Ma (Grenville) peak that suggests detrital zircon was sourced from the Appalachians. Appalachian detrital zircons first appear in the western United States during the Pennsylvanian–Permian (e.g., Ingleside Formation in Colorado Front Range; Nair et al., 2018). The Appalachian-derived detrital zircon could have been recycled from nearby Paleozoic and younger sediments, and our data are not conclusive in distinguishing local from more distant sediment sources.

CONCLUSIONS

This study constrains the Paleocene–Eocene boundary in the rapidly subsiding Hanna Basin and provides a detailed stratigraphic framework of fluvial, paludal, and lacustrine facies across the upper part of the Hanna Formation. Plant fossils and palynology have so far proved to be the most reliable tools to constrain the PETM. Bulk $\delta^{13}C_{org}$ isotopes from carbonaceous shales show most negative values between Coal 82 and 83 in Hanna Draw corresponding with the here-defined PETM; however, bulk $\delta^{13}C_{org}$ isotopes in The Breaks are harder to interpret and need denser sampling. The fluvial response to the PETM in the Hanna Basin as an increased pulse of coarse sediment coincides with sedimentary responses described in other Laramide basins where it is typically attributed to a more seasonal climate. Besides the occurrence of a large sandstone at the PETM, a repetitive pattern of similar large sand bodies alternating with coals exists throughout the Hanna Formation. It remains unknown if this

cyclicity results from autocyclicity common to avulsive systems, drainage capturing, climatic signals such as orbital forcing, or other causes. The only date in our stratigraphic framework is the location of the PETM between Coal 82 and 83. Attempts to add time control with zircons remained inconclusive since the zircons were likely detrital and therefore report depositional ages, rather than absolute ages. Additional efforts to increase resolution in correlations and environmental interpretations, especially in the Eocene part of the section by using mollusks, have so far been unsuccessful due to the poor preservation of specimens and uncertainty tying into regional correlations. More age control would better document timing and rates of sedimentation in the basin.

The identification of the Paleocene–Eocene boundary in the Hanna Basin adds an important spatial data point for comparison of PETM sections in terrestrial basins across the western United States. The abundance of carbonaceous shales improves preservation of paleobotanical material and offers more detailed documentation of changes across the PETM compared to more arid basins, such as the Piceance and Bighorn Basins.

ACKNOWLEDGMENTS

This study was part of the mapping efforts by the U.S. Geological Survey (USGS) National Geologic Mapping Program and National Science Foundation grant EAR-145031 to Currano. Field assistance and discussions by Jenna West, Kristi Zellman, Robin Swank, Lauren Schmidt, Kymbre Skersies, Sarah Fanning, Lukas Lindquist, and Michael Loveland were highly appreciated. Burt and Kay Lynn Palm, the Q-Creek Ranch, Anadarko, Wyoming State lands, and the Bureau of Land Management (BLM) are thanked for land access. Work on BLM land was conducted under permit WY-197. We are thankful to Craig Johnson and Cayce Gulbransen of the USGS for help in the lab and insights with isotope analysis. Jen O' Keefe is thanked for processing and interpreting part of the palynological material. Jeremy Havens is thanked for drafting support and suggestions. Chamberlain was partially supported from Mega-Grant 14.Y26.31.0012 and Science Research project 18-17-00240 of the government of the Russian Federation. Joseph Hartman thanks with appreciation his Hanna Basin museum and field crew Aaron Sobbe and Danielle Zinsmaster of the Harold Hamm School of Geology and Geological Engineering, and Don McCollor and the Energy & Environmental Research Center, at the University of North Dakota (UND). Access to the Gary Glass collections was provided by Laura Vietti, Collections Manager of the Geological Museum, University of Wyoming (UW), and Donald Boyd, Professor Emeritus (UW). Unpublished documents were generously provided by Chris Carroll of the Wyoming State Geological Survey (WGS) and Gary Glass (formerly of WGS). High-resolution images of published material were kindly provided by Jay Lillegraven, Emeritus Professor (UW). Support for this project was provided by the Bud and Mardi Paleontology Fund (UND) and John Reid Fund (UND).

USGS reviewers Debra Higley and Julie Herrick are thanked for helpful comments. Anonymous GSA reviewers and the editors of *Geosphere* are thanked for their helpful and constructive comments to improve this document for publication.

Any use of trade, firm, or product names is for descriptive purposes only and does not imply endorsement by the U.S. Government. All pictures were taken by M. Dechesne, unless otherwise noted.

REFERENCES CITED

Alonso-Zarza, A., 2003, Palaeoenvironmental significance of palustrine carbonates and calcretes in the geological record: Earth-Science Reviews, v. 60, p. 261–298, https://doi.org/10.1016/S0012-8252(02)00106-X.

Amato, J.M., Boullion, A.O., Serna, A.M., Sanders, A.E., Farmer, G.L., Gehrels, G.E., and Wooden, J.L., 2008, Evolution of the Mazatzal province and the timing of the Mazatzal orogeny: Insights from U-Pb geochronology and geochemistry of igneous and metasedimentary rocks in southern New Mexico: Geological Society of America Bulletin, v. 120, p. 328–346, https://doi.org/10.1130/B26200.1.

Aswasereelert, W., Meyers, S.R., Carroll, A.R., Peters, S.E., Smith, M.E., and Feigl, K.L., 2013, Basin-scale cyclostratigraphy of the Green River Formation, Wyoming: Geological Society of America Bulletin, v. 125, p. 216–228, https://doi.org/10.1130/B30541.1.

Baczynski, A.A., McInerney, F.A., Wing, S.L., Kraus, M.J., Morse, P.E., Bloch, J.I., Chung, A.H., and Freeman, K.H., 2016, Distortion of carbon isotope excursion in bulk soil organic matter during the Paleocene–Eocene thermal maximum: Geological Society of America Bulletin, v. 128, p. 1352–1366, https://doi.org/10.1130/B31389.1.

Blackstone, D.L., Jr., 1993, Overview of the Hanna, Carbon, and Cooper Lake Basins, southeastern Wyoming: Geological Survey of Wyoming Report of Investigations, v. 48, p. 1–20.

Bohacs, K., and Suter, J., 1997, Sequence stratigraphic distribution of coaly rocks: Fundamental controls and paralic examples: The American Association of Petroleum Geologists Bulletin, v. 81, p. 1612–1639.

Bowen, C.F., 1918, Stratigraphy of the Hanna Basin, Wyoming: U.S. Geological Survey Professional Paper 108-L, p. 227–235, https://doi.org/10.3133/pp108L.

Bowen, G.J., Beerling, D.J., Koch, P.L., Zachos, J.C., and Quattlebaum, T., 2004, A humid climate state during the Palaeocene/Eocene thermal maximum: Nature, v. 432, p. 495–499, https://doi.org/10.1038/nature03115.

Bowen, G.J., Daniels, A.L., and Bowen, B.B., 2008, Paleoenvironmental isotope geochemistry and paragenesis of lacustrine and palustrine carbonates, Flagstaff Formation, central Utah, USA: Journal of Sedimentary Research, v. 78, p. 162–174, https://doi.org/10.2110/jsr.2008.021.

Bowen, G.J., Maibauer, B.J., Kraus, M.J., Röhl, U., Westerhold, T., Steimke, A., Gingerich, P.D., Wing, S.L., and Clyde, W.C., 2015, Two massive, rapid releases of carbon during the onset of the Palaeocene–Eocene thermal maximum: Nature Geoscience, v. 8, p. 44–47, https://doi.org/10.1038/ngeo2316.

Boyd, D.W., and Lillegraven, J.A., 2011, Persistence of the Western Interior Seaway: Rocky Mountain Geology, v. 46, p. 43–69, https://doi.org/10.2113/gsrocky.46.1.43.

Brown, R.W., 1962, Paleocene flora of the Rocky Mountains and Great Plains: U.S. Geological Survey Professional Paper 375, 269 p., https://doi.org/10.3133/pp375.

Carroll, A.R., and Bohacs, K.M., 1999, Stratigraphic classification of ancient lakes: Balancing tectonic and climatic controls: Geology, v. 27, p. 99–102, https://doi.org/10.1130/0091-7613(1999)027<0099:SCOALB>2.3.CO;2.

Cather, S.M., Chapin, C.E., and Kelley, S.A., 2012, Diachronous episodes of Cenozoic erosion in southwestern North America and their relationship to surface uplift, paleoclimate, paleodrainage, and paleoaltimetry: Geosphere, v. 8, p. 1177–1206, https://doi.org/10.1130/GES00801.1.

Cecil, C.B., 1990, Paleoclimate controls on stratigraphic repetition of chemical and siliciclastic rocks: Geology, v. 18, p. 533–536, https://doi.org/10.1130/0091-7613(1990)018<0533:PCOSRO>2.3.CO;2.

Cole, J.C., Trexler, J.H., Jr., Cashman, P.H., Miller, I.M., Shroba, R.R., Cosca, M.A., and Workman, J.B., 2010, Beyond Colorado's Front Range—A new look at Laramide basin subsidence, sedimentation, and deformation in north-central Colorado, *in* Morgan, L.A., and Quane, S.L., eds., Through the Generations: Geologic and Anthropogenic Field Excursions in the Rocky Mountains from Modern to Ancient: Geological Society of America Field Guide 18, p. 55–76, https://doi.org/10.1130/2010.0018(03).

Colombera, L., Arévalo, O., and Mountney, N., 2017, Fluvial-system response to climate change: The Paleocene–Eocene Tremp Group, Pyrenees, Spain: Global and Planetary Change, v. 157, p. 1–17, https://doi.org/10.1016/j.gloplacha.2017.08.011.

Copeland, P., Currie, C., Lawton, T., and Murphy, M., 2017, Location, location, location: The variable lifespan of the Laramide orogeny: Geology, p. 223–226, https://doi.org/10.1130/G38810.1.

Coplen, T.B., 1994, Reporting of stable hydrogen, carbon, and oxygen isotopic abundances: Pure and Applied Chemistry, v. 66, p. 273-276, https://doi.org/10.1351/pac199466020273.

Cross, T.A., and Pilger, R.H., Jr., 1978, Constraints on absolute motion and plate interaction inferred from Cenozoic igneous activity in the western United States: American Journal of Science, v. 278, p. 865–902, https://doi.org/10.2475/ajs.278.7.865.

Cui, Y., Kump, L.R., Ridgwell, A.J., Charles, A.J., Junium, C.K., Diefendorf, A.F., Freeman, K.H., Urban, N.M., and Harding, I.C., 2011, Slow release of fossil carbon during the Palaeocene–Eocene Thermal Maximum: Nature Geoscience, v. 4, no. 7, p. 481–485, https://doi.org/10.1038/ngeo1179.

Davis, B.S., 2006. Stromatolites in the upper lacustrine unit of the Paleocene Hanna Formation, Hanna Basin, south-central Wyoming [M.S. thesis]: Laramie, University of Wyoming.

Dechesne, M., Cole, J.C., Trexler, J.H., Jr., Cashman, P.H., and Peterson, C.D., 2013, Laramide basin CSI: Comprehensive stratigraphic investigations of Paleogene sediments in the Colorado

Headwaters Basin, north-central Colorado, *in* Abbott, L.D., and Hancock, G.S., eds., Classic Concepts and New Directions: Exploring 125 Years of GSA Discoveries in the Rocky Mountain Region: Geological Society of America Field Guide 33, p. 139–163, https://doi.org/10.1130/2013.0033(04).

Dickinson, W.R., and Snyder, W., 1978, Plate tectonics of the Laramide orogeny, *in* Matthew, V., III, ed., Laramide Folding Associated with Basement Block Faulting in the Western United States: Geological Society of America Memoir 151, https://doi.org/10.1130/MEM151-p355.

Dobbin, C.E., Bowen, C.F., and Hoots, H.W., 1929, Geology and coal and oil resources of the Hanna and Carbons Basins, Carbon County, Wyoming: U.S. Geological Survey Bulletin 804, vi + 88 p.

Duebendorfer, E.M., Chamberlain, K.R., and Fry, B., 2006, Mojave-Yavapai boundary zone, southwestern United States: A rifting model for the formation of an isotopically mixed crustal boundary zone: Geology, v. 34, p. 681–684, https://doi.org/10.1130/G22581.1.

Dunn, R.E., 2003, Correlation of Leaf Megafossil and Palynological Data with North American Land Mammal Ages from Paleocene-Aged Strata of the Ferris and Hanna Formations, Hanna Basin, South-Central Wyoming [M.S. thesis]: Laramie, University of Wyoming, 204 p.

Eberle, J.J., and Lillegraven, J.A., 1998a, A new important record of earliest Cenozoic mammalian history: Geologic Setting, Multituberculata, and Peradectia: Rocky Mountain Geology, v. 33, p. 3–47.

Eberle, J.J., and Lillegraven, J.A., 1998b, Eutheria and paleogeographic/biostratigraphic summaries: Rocky Mountain Geology, v. 33, p. 44–117.

Eldrett, J.S., Greenwood, D.R., Polling, M, Brinkhuis, H., and Sluijs, A., 2014, A seasonality trigger for carbon injection at the Paleocene–Eocene thermal maximum: Climate of the Past, v. 10, p. 759–769, https://doi.org/10.5194/cp-10-759-2014. (NB: amended from and replaces earlier draft in Clim. Past. Discussions in 2013).

Flores, R.M., 1990, Transverse and longitudinal Gilbert-type deltas, Tertiary Coalmont Formation, North Park Basin, Colorado, USA: International Association of Sedimentology Special Publication, v. 19, p. 223–233.

Flores, R.M., 2003, Paleocene paleogeographic, paleotectonic, and paleoclimatic patterns of the northern Rocky Mountains and Great Plains region, *in* Raynolds, R.G., and Flores, R.M., eds., Cenozoic Systems of the Rocky Mountain region: Denver, Colorado, Rocky Mountain Section SEPM (Society for Sedimentary Geology), p. 63–106.

Flores, R.M., Cavaroc, V.V., Ochs, A.M., and Bader, L.R., 1999a, Framework geology of Ferris and Hanna coal in the Hanna and Carbon Basins: U.S. Geological Survey Professional Paper 1625-A, p. 1–45.

Flores, R.M., Cavaroc, V.V., and Bader, L.R., 1999b, Ferris and Hanna coal in the Hanna and Carbon basin, Wyoming: A synthesis *in* Resource assessment of selected Tertiary coal beds and zones in the Northern Rocky Mountains and Great Plains region: U.S. Geological Survey Professional Paper 1625-A, 49 p.

Foreman, B., Heller, P., and Clementz, M., 2012, Fluvial response to abrupt global warming at the Palaeocene/Eocene boundary: Nature, v. 491, p. 92–95, https://doi.org/10.1038/nature11513.

Foreman, B.Z., 2014, Climate-driven generation of a fluvial sheet sand body at the Paleocene–Eocene boundary in north-west Wyoming (USA): Basin Research, v. 26, no. 2, p. 225–241, https://doi.org/10.1111/bre.12027.

Galloway, W.E., Whiteaker, T.L. and Ganey-Curry, P., 2011, History of Cenozoic North American drainage basin evolution, sediment yield, and accumulation in the Gulf of Mexico basin: Geosphere, v. 7, p. 938–973, https://doi.org/10.1130/GES00647.1.

Gill, J.R., Merewether, E.A., and Cobban, W.A., 1970, Stratigraphy and nomenclature of some Upper Cretaceous and lower Tertiary rocks in south-central Wyoming: U.S. Geological Survey Professional Paper 667, 53 p., https://doi.org/10.3133/pp667.

Gingerich, P.D., and Clyde, W.C., 2001, Overview of mammalian biostratigraphy in the Paleocene–Eocene Fort Union and Willwood Formations of the Bighorn and Clarks Fork Basins, *in* Gingerich, P.D., ed., Paleocene–Eocene Stratigraphy and Biotic Change in the Bighorn and Clarks Fork Basins, Wyoming: University of Michigan Papers on Paleontology 33, p. 1–14.

Glass, G.B., 1980, Coals and coal-bearing rocks of the Hanna Coal Field, Wyoming: Wyoming State Geological Survey Report of Investigations 22, iv + 43 p.

Glass, G.B., and Roberts, J.T., 1984, Analysis and Measured Sections of 25 Coal Samples from the Hanna Coal Field of Southcentral Wyoming: Wyoming State Geological Survey Report of Investigations 27, 104 p.

Hajek, E.A., Heller, P.L., and Schur, E.L., 2012, Field test of autogenic control on alluvial stratigraphy (Ferris Formation, Upper Cretaceous–Paleogene, Wyoming): Geological Society of America Bulletin, v. 124, p. 1898–1912, https://doi.org/10.1130/B30526.1.

Harrington, G., Boomer, I., Campion, N., Hughes, G., Jakeman, M., DeVille de Goyet, F., Polling, M., and Cornick, P., 2015, Palynology of the Paleocene–Eocene boundary in the Wilcox Group at the Red Hot Truck Stop, eastern Gulf of Mexico, USA: Geological Society of America Abstracts with Programs, v. 47, p. 61.

Harrington, G.J., 2003a, Geographic patterns in the floral response to Paleocene–Eocene warming, *in* Wing, S.L., Gingerich, P.D., Schmitz, B., and Thomas, E., eds., Causes and Consequences of Globally Warm Climates in the Early Paleogene: Geological Society of America Special Paper 369, p. 381–394, https://doi.org/10.1130/0-8137-2369-8.381.

Harrington, G.J., 2003b, Wasatchian (Early Eocene) pollen floras from the Red Hot Truck Stop, Mississippi, USA: Palaeontology, v. 46, p. 725–738, https://doi.org/10.1111/1475-4983.00318.

Hartman, J.H., 1984, Systematics, biostratigraphy, and biogeography of latest Cretaceous and early Tertiary Viviparidae (Mollusca, Gastropoda) of southern Saskatchewan, western North Dakota, eastern Montana, and northern Wyoming [Ph.D. thesis]: Minneapolis, University of Minnesota, 928 p.

Hartman, J.H., and Roth, B., 1997, Correlation of nonmarine molluscan faunal change during the late Paleocene and early Eocene of the Bighorn and Powder River Basins, Wyoming and Montana: Geological Society of America Abstracts with Programs, v. 29, no. 6, p. A-100.

Hartman, J.H., and Roth, B., 1998, Late Paleocene and early Eocene nonmarine molluscan faunal change in the Bighorn Basin, northwestern Wyoming and south-central Montana, *in* Aubry, M.-P., et al., eds., Late Paleocene–Early Eocene Climatic and Biotic Events in the Marine and Terrestrial Records: New York, Columbia University Press, p. 323–379.

Hasiotis, S.T., and Honey, J.G., 2000, Paleohydrologic and stratigraphic significance of crayfish burrows in continental deposits: Examples from several Paleocene Laramide basins in the Rocky Mountains: Journal of Sedimentary Research, v. 70, p. 127–139, https://doi.org/10.1306/2DC40904-0E47-11D7-8643000102C1865D.

Higgins, P., 2003, A Wyoming succession of Paleocene mammal-bearing localities bracketing the boundary between the Torrejonian and Tiffanian North American Land Mammal "Ages": Rocky Mountain Geology, v. 38, p. 247–280, https://doi.org/10.2113/gsrocky.38.2.247.

Higgins, P., 2012, Climate change at the Paleocene-Eocene boundary: New insights from mollusks and organic carbon in the Hanna Basin of Wyoming: Palarch's Journal of Vertebrate Palaeontology, v. 9, p. 1–20.

Jaramillo, C., Ochoa, D., Contreras, L., Pagani, M., Carvajal-Ortiz, H., Pratt, L.M., and Vervoort, J., 2010, Effects of rapid global warming at the Paleocene–Eocene boundary on neotropical vegetation: Science, v. 330, p. 957–961, https://doi.org/10.1126/science.1193833.

Johnson, C.A., Stricker, C.A., Gulbransen, C.A., and Emmons, M.P., 2018, Determination of $\delta^{13}C$, $\delta^{15}N$, or $\delta^{34}S$ by isotope-ratio-monitoring mass spectrometry using an elemental analyzer: U.S. Geological Survey Techniques and Methods, book 5, chap. D4, 19 p., https://doi.org/10.3133/tm5D4.

Jolley, D.W., 1997, Palaeosurface palynofloras of the Skye lava field and age of the British Tertiary volcanic province, *in* Widdowson, M., ed., Palaeosurfaces: Recognition, Reconstruction, and Palaeoenvironmental Interpretation: Geological Society of London Special Publication 120, p. 67–94, https://doi.org/10.1144/GSL.SP.1997.120.01.06.

Jones, C., Farmer, L., Sageman, B., and Zhong, S., 2011, Hydrodynamic mechanism for the Laramide orogeny: Geosphere, v. 7, p. 183–201, https://doi.org/10.1130/GES00575.1.

Kennett, J.P., and Stott, L.D., 1991, Abrupt deep-sea warming, palaeoceanographic changes and benthic extinctions at the end of the Palaeocene: Nature, v. 353, p. 225–229, https://doi.org/10.1038/353225a0.

Kirschner, W.A., 1984, Non-marine molluscan paleontology and paleoecology of early Tertiary strata, Hanna Basin, Wyoming [M.S. thesis]: Laramie, University of Wyoming, 157 p.

Knight, S.H., 1951, The late Cretaceous–Tertiary history of the northern portion of the Hanna basin, Carbon County, Wyoming, *in* Wyoming Geological Association Guidebook, 6th Annual Field Conference, south-central Wyoming: Laramie, p. 45–53.

Koch, P.L., Zachos, J.C., and Gingerich, P.D., 1992, Correlation between isotope records in marine and continental carbon reservoirs near the Palaeocene/Eocene boundary: Nature, v. 358, p. 319–322, https://doi.org/10.1038/358319a0.

Kraatz, B.P., 2002, Structural and seismic-reflection evidence for development of the Simpson Ridge anticline and separation of the Hanna and Carbon Basins, Carbon County, Wyoming: Rocky Mountain Geology, v. 37, p. 75–96, https://doi.org/10.2113/gsrocky.37.1.75.

Kraus, M.J., McInerney, F.A., Wing, S.L., Secord, R., Baczynski, A.A., and Bloch, J.I., 2013, Paleohydrologic response to continental warming during the Paleocene–Eocene Thermal Maximum, Bighorn Basin, Wyoming: Palaeogeography, Palaeoclimatology, Palaeoecology, v. 370, p. 196–208, https://doi.org/10.1016/j.palaeo.2012.12.008.

Kraus, M.J., Woody, D.T., Smith, J.J., and Dukic, V., 2015, Alluvial response to the Paleocene–Eocene Thermal Maximum climatic event, Polecat Bench, Wyoming (U.S.A.): Palaeogeography, Palaeoclimatology, Palaeoecology, v. 435, p. 177–192, https://doi.org/10.1016/j.palaeo.2015.06.021.

La Rocque, A., 1960, Molluscan Faunas of the Flagstaff Formation of Central Utah: Geological Society of America Memoir 78, 100 p., https://doi.org/10.1130/MEM78-p1.

LeFebre, G.B., 1988, Tectonic evolution of the Hanna Basin, Wyoming: Laramide block rotation in the Rocky Mountain foreland [Ph.D. thesis]: Laramie, University of Wyoming, 240 p.

Lesquereux, L., 1874, Contributions to the fossil flora western territories, Part I. the Cretaceous flora, *in* Hayden, F.V., U.S. Geologist-in-Charge, Report of the United States Geological Survey of the Territories [Monograph]: Washington, D.C., Government Printing Office, v. VI, p. 1–136, pls. I–XXX.

Lillegraven, J.A., 1994, Age of upper reaches of Hanna Formation, northern Hanna Basin, south-central Wyoming: Berliner geowissenschaftliche Abhandlungen, Reihe E (Paläobiologie), Band 13 (B. Krebs-Festschrift), p. 203–219.

Lillegraven, J.A., 2015, Late Laramide tectonic fragmentation of the eastern greater Green River Basin, Wyoming: Rocky Mountain Geology, v. 50, p. 30–118, https://doi.org/10.2113/gsrocky.50.1.30.

Lillegraven, J.A., and Snoke, A.W., 1996, A new look at the Laramide orogeny in the Seminoe and Shirley Mountains, Freezeout Hills, and Hanna Basin, south-central Wyoming: Geological Survey of Wyoming Public Information Circular, no. 36, ii + 56 p.

Lillegraven, J.A., Snoke, A.W., and McKenna, M.C., 2004, Tectonic and paleogeographic implications of late Laramide geologic history in the northeastern corner of Wyoming's Hanna Basin: Rocky Mountain Geology, v. 39, p. 7–64, https://doi.org/10.2113/gsrocky.39.1.7.

Loope, D., and Secord, R., 2017, Interactions of a Paleocene river, a rising fold, and early-diagenetic concretions: Journal of Sedimentary Research, v. 87, p. 866–879, https://doi.org/10.2110/jsr.2017.52.

Love, J.D., and Christiansen, A.C., 1985, Geologic map of Wyoming: U.S. Geological Survey, scale 1:500,000.

Ludwig, K.R., 1998, On the treatment of concordant uranium-lead ages: Geochimica et Cosmochimica Acta, v. 62, p. 665–676, https://doi.org/10.1016/S0016-7037(98)00059-3.

Lyons, S., Baczynski, A., Vornlocher, J., Polites, E., and Freeman, K., 2017, Destabilization of carbon on land, and coastal ocean response during the PETM: Evidence from mid-Atlantic sediments: Climatic and Biotic Events of the Paleogene conference, September 2017.

Manchester, S.R., 1987, The fossil history of the Juglandaceae: Missouri Botanical Garden Monographs, v. 21, p. 1–137.

Manchester, S.R., and Zavada, M.S., 1987, Lygodium foliage with intact sorophores from the Eocene of Wyoming: Chicago, Illinois, Botanical Gazette, v. 148, p. 392–399, https://doi.org/10.1086/337668.

Manchester, S.R., Xiang, Q.-Y., Kodrul, T.M., and Akhmetieyz, M.A., 2009, Leaves of Cornus (Cornaceae) from the Paleocene of North America and Asia confirmed by trichome characters: International Journal of Plant Sciences, v. 170, p. 132–142, https://doi.org/10.1086/593040.

Mattinson, J.M., 2005, Zircon U-Pb chemical abrasion ("CA-TIMS") method: Combined annealing and multi-step partial dissolution analysis for improved precision and accuracy of zircon ages: Chemical Geology, v. 220, p. 47–66, https://doi.org/10.1016/j.chemgeo.2005.03.011.

McCabe, P.J., 1984, Depositional models of coal and coal-bearing strata, *in* Rahmani, R.A., and Flores, R.M., eds., Sedimentology of Coal and Coal-bearing Sequences: International Association of Sedimentologists, Special Publication 7, p. 13–42.

McInerney, F.A., and Wing, S.L., 2011, The Paleocene–Eocene Thermal Maximum: A perturbation of carbon cycle, climate, and biosphere with implications for the future: Annual Review of Earth and Planetary Sciences, v. 39, p. 489–516, https://doi.org/10.1146/annurev-earth-040610-133431.

National Agriculture Imagery Program (NAIP), 2012, Aerial photography at 1 m resolution: Carbon County, Wyoming, fsa.usds.gov (last accessed October 2018).

Nair, K., Holm-Denoma, C.S., Singleton, J., and Egenhoff, S., 2018, Detrital zircon geochronology of Pennsylvanian–Permian strata in Colorado: Evidence for Appalachian-derived sediment and implications for the timing of Ancestral Rocky Mountains uplift: The Mountain Geologist, v. 55, p. 119–140, https://doi.org/10.31582/rmag.mg.55.3.119.

Nichols, D.J., 2003, Palynostratigraphic framework for age determination and correlation of the nonmarine lower Cenozoic of the Rocky Mountains and Great Plains region, *in* Raynolds, R.G., and Flores, R.M., eds., Cenozoic Systems of the Rocky Mountain Region: Rocky Mountain Section of the Society for Sedimentary Geology (SEPM), Denver, p. 107–134.

Nichols, D.J., and Ott, H.L., 1978, Biostratigraphy and evolution of the Momipites—Caryapollenites lineage in the early Tertiary in the Wind River Basin, Wyoming: Palynology, v. 2, p. 93–112, https://doi.org/10.1080/01916122.1978.9989167.

Noorbergen, L.J., Abels, H.A., Hilgen, F.J., Robson, B.E., de Jong, E., Dekkers, M.J., Krijgsman, W., Smit, J., Collinson, M.E., and Kuiper, K.F., 2017, Conceptual models for short-eccentricity-scale climate control on peat formation in a lower Palaeocene fluvial system, north-eastern Montana (USA): Sedimentology, v. 65, no 3, p. 775–808, https://doi.org/10.1111/sed.12405.

O'Keefe, J.M.K., and Eble, C.F., 2012, A comparison of HF-based and non-HF-based palynology processing techniques in clay-rich lignites from the Claiborne Group, upper Mississippi Embayment, United States: Palynology, v. 36, p. 116–130, https://doi.org/10.1080/01916122.2011.642484.

Payros, A., Ortiz, S., Millán, I., Arostegi, J., Orue-Etxebarria, X., and Apellaniz, E., 2015, Early Eocene climatic optimum: Environmental impact on the North Iberian continental margin: Geological Society of America Bulletin, v. 127, p. 1632–1644, https://doi.org/10.1130/B31278.1.

Perry, W.J., and Flores, R.W., 1997, Sequential Laramide deformation and Paleocene depositional patterns in deep gas-prone basins of the Rocky Mountain region, *in* Dyman, T.S., Rice, D.D., and Westcott, P.A., eds., Geologic Controls of Deep Natural Resources in the United States: U.S. Geological Survey Bulletin 2146, p. 49–59.

Pew, C.R., 2014, The Paleocene Eocene Thermal Maximum in the Hanna Basin, WY: Constraints from Organic Carbon Isotopes and Palynological Data [M.S. thesis]: Seattle, University of Washington.

Peyton, L.S, and Carrapa, B., 2013, An overview of low-temperature thermochronology in the Rocky Mountain and Its application to petroleum system analysis, *in* Knight, C., and Cuzella, J., eds., Application of Structural Methods to Rocky Mountain Hydrocarbon Exploration and Development: AAPG Studies in Geology, v. 65, p. 37–70.

Pierce, B.S., 1996, Quality and petrographic characteristics of Paleocene coals from the Hanna Basin, Wyoming, *in* Stanton, R., ed., Collected Papers from The Twelfth Annual Meeting of the Society for Organic Petrology: Organic Geochemistry, v. 24, p. 181–187.

Plink-Björklund, P., 2015, Morphodynamics of rivers strongly affected by monsoon precipitation: Review of depositional style and forcing factors: Sedimentary Geology, v. 323, p. 110–147, https://doi.org/10.1016/j.sedgeo.2015.04.004.

Raynolds, R.G., and Johnson, K.R., 2003, Synopsis of the stratigraphy and paleontology of the uppermost Cretaceous and lower Tertiary strata in the Denver Basin, Colorado: Rocky Mountain Geology, v. 38, no. 1, p. 171–181, https://doi.org/10.2113/gsrocky.38.1.171.

Roberts, L.N.R., and Kirschbaum, M.A., 1995, Paleogeography of the Late Cretaceous of the Western Interior of middle North America—Coal distribution and sediment accumulation: U.S. Geological Survey Professional Paper 1561, 155 p., https://doi.org/10.3133/pp1561.

Rocky Mountain Association of Geologists (RMAG), 2014, Tectonic GIS Data from the Geologic Atlas of the Rocky Mountain Region: Denver, Colorado, Rocky Mountain Association of Geologists, CD-ROM.

Ryan, J.D., 1977, Late Cretaceous and early Tertiary provenance and sediment dispersal, Hanna and Carbon Basins, Carbon County, Wyoming: Geological Survey of Wyoming Preliminary Report 16, 17 p.

Secord, R., 1998, Paleocene mammalian biostratigraphy of the Carbon Basin, southeastern Wyoming, and age constraints on local phases of tectonism: Rocky Mountain Geology, v. 33, p. 119–154.

Sharman, G.R., Covault, J.A., Stockli, D.F., Wroblewski, A.F., and Bush, M.A., 2017, Early Cenozoic drainage reorganization of the United States Western Interior–Gulf of Mexico sediment routing system: Geology, v. 45, p. 187–190, https://doi.org/10.1130/G38765.1.

Sluijs, A., van Roij, L., Harrington, G.J., Schouten, S., Sessa, J.A., LeVay, L.J., Reichart, G.-J., and Slomp, C.P., 2014, Warming, euxinia and sea level rise during the Paleocene–Eocene Thermal Maximum on the Gulf Coastal Plain: Implications for ocean oxygenation and nutrient cycling: Climate of the Past, v. 10, p. 1421–1439, https://doi.org/10.5194/cp-10-1421-2014.

Smith, M.E., Carroll, A.R., and Singer, B.S., 2008, Synoptic reconstruction of a major ancient lake system: Eocene Green River Formation, western United States: Geological Society of America Bulletin, v. 120, p. 54–84, https://doi.org/10.1130/B26073.1.

Smith, M.E., Carroll, A.R., Scott, J.J., and Singer, B.S., 2014a, Early Eocene carbon isotope excursions and landscape destabilization at eccentricity minima: Green River Formation of Wyoming: Earth and Planetary Science Letters, v. 403, p. 393–406, https://doi.org/10.1016/j.epsl.2014.06.024.

Smith, M.E., Carroll, A.R., Jicha, B.R., Cassel, E.J., and Scott, J.J., 2014b, Paleogeographic record of Eocene Farallon slab rollback beneath western North America: Geology, v. 42, p. 1039–1042, https://doi.org/10.1130/G36025.1.

Smith, M.E., Carroll, A.R., and Scott, J.J., 2015a, Stratigraphic expression of climate, tectonism, and geomorphic forcing in an underfilled lake basin: Wilkins Peak Member of the Green River Formation, *in* Smith, M.E., and Carroll, A.R., eds., Stratigraphy and Paleolimnology of the Green River Formation, Western USA: Springer, Dordrecht, p. 61–102, https://doi.org/10.1007/978-94-017-9906-5_4.

Smith, M.E., Jicha, B.R., Carroll, A.R., Cassel, E.J., and Scott, J.J., 2015b, Paleogeographic record of Eocene Farallon slab rollback beneath western North America: Reply to Discussion: Geology, v. 43, p. e364, https://doi.org/10.1130/G36878Y.1.

Stanton, T.W., 1916, (7 Mar.) (unpublished), Letter report for C.F. Bowen on invertebrate fossils from Hanna and Saddleback Hills Quadrangles, Wyoming: Washington, D.C., U.S. Geological Survey Correspondence, 9 p.

Veatch, A.C., 1907, Geography and Geology of a Portion of Southwestern Wyoming, with Special Reference to Coal and Oil: U.S. Geological Survey Professional Paper 56, 178 p., https://doi.org/10.3133/pp56.

Westerhold, T., Röhl, U., Laskar, J., Raffi, I., Bowles, J., Lourens, L., Zachos, J., Westerhold, T., Röhl, U., Laskar, J., Raffi, I., Bowles, J., Lourens, L., and Zachos, J., 2007, On the duration of magnetochrons C24r and C25n and the timing of early Eocene global warming events: Implications from the Ocean Drilling Program Leg 208 Walvis Ridge depth transect: Paleoceanography, v. 22, no. 2, https://doi.org/10.1029/2006PA001322.

Wilf, P., 2000, Late Paleocene–early Eocene climate changes in southwestern Wyoming: Paleobotanical analysis: Geological Society of America Bulletin, v. 112, p. 292–307, https://doi.org/10.1130/0016-7606(2000)112<292:LPECCI>2.0.CO;2.

Wing, S., Harrington, G., Smith, F., Bloch, J., Boyer, D., and Freeman, K., 2005, Transient floral change and rapid global warming at the Paleocene–Eocene boundary: Science, v. 310, p. 993–996, https://doi.org/10.1126/science.1116913.

Wing, S.L., 1998, Late Paleocene–early Eocene floral and climatic change in the Bighorn Basin, Wyoming, *in* Aubry, M.P., Lucas, S.G., and Berggren, W.A., eds., Late Paleocene–early Eocene climatic and biotic events in the marine and terrestrial records: New York, Columbia University Press, p. 380–400.

Wing, S.L., and Currano, E.D., 2013, Plant response to a global greenhouse event 56 million years ago: American Journal of Botany, v. 100, p. 1234–1254, https://doi.org/10.3732/ajb.1200554.

Wing, S.L., and Greenwood, D.R., 1993, Fossils and fossil climate: The case for equable continental interiors in the Eocene: Philosophical Transactions of the Royal Society of London. Series B, Biological Sciences, v. 341, p. 243–252, https://doi.org/10.1098/rstb.1993.0109.

Wing, S.L., Harrington, G.J., Bowen, G.J., and Koch, P.L., 2003, Floral change during the Initial Eocene Thermal Maximum in the Powder River Basin, Wyoming, *in* Wing, S.L., Gingerich, P.D., Schmitz, B., and Thomas, E., eds., Causes and Consequences of Globally Warm Climates in the Early Paleogene: Geological Society of America Special Paper 369, p. 425–440, https://doi.org/10.1130/0-8137-2369-8.425.

Winguth, A., Shellito, C., Shields, C., and Winguth, C., 2010, Climate response at the Paleocene–Eocene thermal maximum to greenhouse gas forcing—A model study with CCSM3: Journal of Climate, https://doi.org/10.1175/2009JCLI3113.1.

WOGCC, Wyoming Oil and Gas Conservation Commission well log database, 2016, http://wogcc.wyo.gov/ (accessed July 2016).

Wroblewski, A.F.-J., 2002, The role of the Hanna Basin in revised paleogeographic reconstructions of the Western Interior Sea during the Cretaceous–Tertiary transition, *in* Horn, M.S., ed., Wyoming Geological Association Guidebook: 2002 Field Conference "Wyoming Basins" and 2003 Field Conference, p. 17–40.

Wroblewski, A.F.-J., 2003, Tectonic redirection of Paleocene fluvial drainage systems and lacustrine flooding in the Hanna Basin area, south-central Wyoming, *in* Raynolds, R.G., and Flores, R.M., eds., Cenozoic Systems of the Rocky Mountain Region: Denver, Rocky Mountain Section SEPM (Society for Sedimentary Geology), p. 227–252.

Wroblewski, A.F.J., 2004, New Selachian Paleofaunas from "Fluvial" Deposits of the Ferris and Lower Hanna Formations (Maastrichtian–Selandian: 66–58 Ma): Southern Wyoming: PALAIOS, v. 19, p. 249–258, https://doi.org/10.1669/0883-1351(2004)019<0249:NSPFFD>2.0.CO;2.

Zachos, J.C., Dickens, G.R., and Zeebe, R.E., 2008, An early Cenozoic perspective on greenhouse warming and carbon-cycle dynamics: Nature, v. 451, p. 279–283, https://doi.org/10.1038/nature06588.